Sensors and Prognostics to Mitigate Bleed Air Contamination Events

2012 Progress Report

R.A. Overfelt, B.W. Jones*, S.M. Loo[#], R.L. Haney, A.J. Neer, J.R. Andress, X. Yang, A. Zitova, B.C. Prorok, J.W. Fergus, A.L. Simonian, Joshua Kiepert[#], Michael Pook[#] and Mike Anderson[#]
National Air Transportation Center of Excellence for
Research in the Intermodal Transport Environment (RITE)
Airliner Cabin Environment Research Program
Auburn University
Auburn, AL 36849

*Kansas State University
Manhattan, KS 66506

[#]Boise State University
Boise, ID 83725

April 2012

Report No. RITE-ACER-CoE-2012-05

NOTICE

This work was funded by the U.S Federal Aviation Administration
Office of Aerospace Medicine under
Cooperative Agreement 10-C-RITE.

This publication is available in full-text from
the publications Web site of the
National Air Transportation Center of Excellence for
Research in the Intermodal Transport Environment (RITE) at:
www.acer-coe.org

Technical Report Documentation Page

1. Report No. RITE-ACER-CoE-2012-TBD	2. Government Accession No.	3. Recipient's Catalog No.
4. Title and Subtitle Sensors and Prognostics to Mitigate Bleed Air Contamination Events - 2012 Progress Report		5. Report Date April 27, 2012 6. Performing Organization Code
7. Author(s) R.A. Overfelt, B.W. Jones*, S.M. Loo#, R.L. Haney, A.J. Neer, J.R. Andress, X. Yang, A. Zitova, W. Kilpatrick, B.C. Prorok, J.W. Fergus, A.L. Simonian, Joshua Kiepert#, Michael Pook# and Mike Anderson#		8. Performing Organization Report No.
9. Performing Organization Name and Address National Air Transportation Center of Excellence for Research in the Intermodal Transport Environment Auburn University Auburn, AL 36849 * Kansas State University Manhattan, KS 66506 # Boise State University Boise, ID 83725		10. Work Unit No. (TRAIS) 11. Contract or Grant No. FAA Cooperative Agreement 10-C-RITE
12. Sponsoring Agency name and Address FAA Office of Aerospace Medicine 800 Independence Ave., S.W. Washington, DC 20591		13. Type of Report and Period Covered 14. Sponsoring Agency Code

15. Supplemental Notes

Work was accomplished under Public law 108-76.

16. Abstract

Most environmental control systems on commercial airliners receive fresh outside air from the bleed air systems of the compressors of the jet engines or from the auxiliary power units. Although outside air is clean and sterile during cruise conditions at flight altitudes, spurious air contamination events have been reported. Bleed air supplies can be contaminated during ground operations by de-icing fluids entering the bleed air supply. Engine oil from worn mechanical seals and hydraulic fluids have also been reported to contaminate the bleed air supply. This document provides an interim Progess Report on a project that is evaluating the applicability of commercial air quality sensing technologies that may provide: (i) accurate, reliable, in-flight detection of bleed air contamination incidents, (ii) real-time determination of root causes of air contamination incidents to facilitate corrective or adaptive action in-flight, (iii) pre-incident detection and reporting to enable preventative maintenance, and (iv) post incident reporting and assessment of recorded information to enable appropriate corrective maintenance actions.

17. Key Words	18. Distribution Statement		
Sensors, aircraft, bleed air, contamination, data mining			
19. Security Classif. (of this report) Unclassified	20. Security Classif. (of this page) Unclassified	21. No. of Pages	22. Price

Form DOT F 1700.7 (8-72) Reproduction of completed page authorized

CONTENTS

Nomenclature

AIDS = Accident/Incident Data System
amu = atomic mass unit
APU = auxiliary power unit
ASHRAE = American Society of Heating, Refrigeration and Air-Conditioning Engineers
ASIAS = Aviation Safety Information Analysis and Sharing
ASRS = Aviation Safety Reporting System
BP = British Petroleum
C = Celsius
CFR = Code of Federal Regulations
CO = carbon monoxide
CO_2 = carbon dioxide
DOT = Department of Transportation
DTA = differential thermal analysis
EPA = Environmental Protection Agency
eV = electron volts
FAA = Federal Aviation Administration
FAR = Federal Aviation Regulation
FTIR = Fourier Transform Infra-red
GC = gas chromatography
HVAC = heating, ventilating and air conditioning
IR = infrared
L = liter
M = molar
MEMS = microelectromechanical system
mg = milligram (10^{-3} g)
min = minute
mL = milliliter (10^{-3} L)
MOS = metal oxide semiconductor
MPa = mega-Pascal (10^{6} Pa)
MS = mass spectrometry
NAAQS = National Ambient Air Quality Standards
NASA = National Aeronautics and Space Administration
NDIR = non-dispersive infrared
O_2 = oxygen
O_3 = ozone
OSHA = Occupational Safety and Health Agency
PEL = permissible exposure limit
PID = photoionization detector
PM2.5 = particulate matter less than 2.5 X 10^{-6} m (2.5 microns) in diameter
PM10 = particulate matter less than 10 X 10^{-6} m (10 microns) in diameter
PMMA = polymethyl methacrylate
ppbv = parts per billion by volume
ppm = parts per million
ppmv = parts per million by volume

SDRs = Service Difficulty Reports
SDRS = Service Difficulty Reporting System
SnO_2 = tin oxide
SQL = Structured Query Language
TCP = tri-cresyl phosphate
TGA = thermogravimetric analysis
UV = ultraviolet
VOC = volatile organic compound

$\mu g/m^3$ = 10^{-6} g per cubic meter
μL = 10^{-6} L

List of Tables

List of Figures

1.0 Background and Introduction

As originally granted in the U.S. Federal Aviation Act of 1958 (Public Law 85-726), regulatory authority over the operation of civil aircraft in the United States resides in the Federal Aviation Administration (FAA). The Occupational Safety and Health (OSH) Act of 1970 (Public Law 91-596) was subsequently passed to ensure safe and healthful workplaces across the country. Federal agencies were allowed the authority to exercise jurisdiction over their own workers, and in 1975, the FAA asserted its jurisdiction over the safety and health of cockpit and cabin crews within operating civil aircraft (40 FR 29114, DOT). Since then, the FAA has been authorized to also protect the safety and health of passengers (49 USC 40101D and 40 USC 44701A).

The Federal Aviation Regulations (FARs) implement the FAA's various safety and health requirements. Relevant aspects for the design and operation of commercial aircraft are contained in "Title 14 - Aeronautics and Space" of the Code of Federal Regulations (i.e., 14 CFR). Part 25 of 14 CFR provides the aircraft design standards for transport category airplanes while Part 121 of 14 CFR contains the operating requirements for air carriers and commercial operators.

These regulations provide the FAA's air quality standards with respect to aircraft cabin ventilation and pressure as well as maximum amounts of potential air quality contaminants. Airliner cabins are typically supplied outside air at rates of about 8-16 cfm per passenger and total air exchanges average approximately 15-25 cabin air exchanges per hour [1]. Table I compares the federal ambient air quality standards of the EPA with OSHA's corresponding workplace standards and the FAA limits for aircraft. While 14 CFR 25.831 states that aircraft air must be free from harmful or hazardous concentrations of gases or vapors and 14 CFR 121.219 notes that fuel fumes may not be present in the air, the FAA specifically only limits the following: (i) ozone, (ii) carbon monoxide and (iii) carbon dioxide. Even with specific allowable limits, there are no requirements for real-time monitoring of any of these contaminants on an aircraft.

Aircraft air supplies can be contaminated during ground operations by exhaust fumes from the engines of nearby aircraft or perhaps by de-icing fluids entering the outside air supply. One example of such an event occurred in December 2008 when de-icer fumes entered the cabin of an Alaskan Airlines plane. Seven crew members were sent to the hospital and 18 passengers were treated on-sight for eye irritation, dizziness, and nausea [2]. Although outside air is clean and sterile during cruise conditions at flight altitudes, spurious air contamination events have also been reported during flight [1, 3-5] due to engine oils and/or hydraulic fluids from worn mechanical seals or overfilled sumps. For example, a suspected hydraulic fluid leak in January 2010 on a U.S. Airways flight is believed responsible for fumes entering the cabin of the airplane. Passengers and crew members complained of headaches and nausea [5]. Engine oil contamination of the air supply is particularly worrisome since some engine oils contain 1-5% tricresyl phosphate, a wear-reduction additive and potential health hazard [6,7]. Given the very high air flow rates and high temperatures in the upstream portion of the bleed air system, the specific nature and extent of potential decomposition reactions of engine oils and hydraulic fluids are largely unknown. In addition, the resulting nature and potential toxicity of any contaminants in the aircraft cabin from such events are highly speculative at the present time.

Table I
Applicable Air Quality Standards: Ambient Air, Workplaces and Aircraft

Pollutant	*Ambient Standard EPA NAAQS 40 CFR*	*Workplace Standard OSHA PEL*	*Aircraft Standard FAA - 14 CFR*
Ozone	0.12 ppmv 1-hr 0.08 ppmv 8-hr	0.1 ppmv	0.1 ppmv* 0.25 ppmv**
Carbon Monoxide	35 ppmv 1-hr 9 ppmv 8-hr	50 ppmv	50 ppmv#
Carbon Dioxide	NA	5000 ppmv	5000 ppmv#
PM_{10}	150 $\mu g/m^3$ 24-hr	NA	NA
$PM_{2.5}$	65 $\mu g/m^3$ 24-hr	NA	NA

* "0.1 parts per million by volume, sea level equivalent, time weighted average during any 3-hr interval" – 14 CFR 25.832
** "0.25 parts per million by volume, sea level equivalent, at any time above 32,000 ft" – 14 CFR 25.832
# - 14 CFR 25.831

In 2009 Watson conducted an internal FAA review of records to ascertain the number of bleed air contamination events within the domestic air transportation system [8]. The FAA Aviation Safety Information Analysis and Sharing (ASIAS) system is composed of multiple databases including the Accident/Incident Data System (AIDS) and the Service Difficulty Reporting System (SDRS). The FAA review of the SDRS database covered January 1999 - November 2008 and looked for event records that noted the following identification terms: "odor, smell or fume." The search found 252 air contamination events where failures occurred in "airplane, engine or auxiliary power unit systems that may have caused tri-cresyl phosphate lubricants or phosphate ester hydraulic fluids or fuel or products of combustion of these fluids to enter the cockpit/cabin ventilation systems." Of these 252 reported incidents, 33% were due to fuel leaks, 23% were from propulsion engine oil leaks, 18% were from APU oil leaks, 13% were due to air cycle machine oil leaks and 13% were due to hydraulic fluid leaks. During this same period of time, there were 93,647,734 corresponding aircraft departures. Thus the event rate is of the order of 2.7 events per million aircraft departures. Watson noted the "trial-and-error" nature of maintenance diagnostics for such events. In several cases, multiple events were recorded in the SDRS database for the same aircraft before the problem was properly diagnosed and then satisfactorily resolved by maintenance crews.

Murawski and Supplee [9] examined the AIDS and SDRS databases over an 18 month period from January 2006 through June 2007. These researchers supplemented the federal databases with additional data from aircraft flight attendant labor union records as well as publically available newspaper reports. Their search looked for records containing the following complaint terms: fume, haze, mist, odor, smell or smoke. In addition, the search also included reports of engine oil maintenance issues that did not explicitly mention an air contamination issue. (It is unclear how the authors decided to include such records into their data set.) Murawski and Supplee concluded that 0.86 events occurred each day during the 18 month study period. With approximately 26,060 U.S. aircraft departures per day in 2006 [10], the event rate for 2006 was estimated to be of the order of 33 events per million aircraft departures. This finding is about an order of magnitude greater that that found by Watson [8].

In 2008, the American Society of Heating, Refrigeration and Air-Conditioning Engineers (ASHRAE) published ASHRAE Standard 161-2007, "Air Quality within Commercial Aircraft" [10]. The standard discusses at length multiple possible sources of air contamination on aircraft and mandates installation of "one or more" sensors to detect "partly or fully pyrolized engine oil or hydraulic fluid" in the bleed air system. However, the standard does not define specifically what should be monitored nor how it should be monitored. Research is needed to establish that specific chemical air contaminants can be identified that are indicative of a bleed air contamination event and that sensor technologies can be developed to reliably detect such events.

2.0 Review of Previous Research

2.1 Overview of Aircraft Bleed Air Supply Systems

An airliner environmental control system (ECS) is designed to (i) pressurize the cabin, (ii) regulate the temperature of the aircraft within acceptable limits of comfort and safety, (iii) provide fresh air to the occupants, (iv) flush gaseous air contaminants overboard and, to some extent, (v) control humidity in the air supply. Except for the new Boeing 787, most aircraft environmental control systems are designed for constant volumetric flow during flight. In addition, the systems often utilize approximately 30-55% re-circulated air to maximize energy efficiency and receive fresh outside air from the bleed air systems of the compressors of the propulsion engines. Typical aircraft systems are not designed for multiple modes of operation (e.g., proportional control) and are either simply ON or OFF. Although the re-circulated air is often filtered with high-efficiency particulate filters that capture 99.7% of all particles larger than 0.3 μm, the reliance on re-circulated air in aircraft to meet ventilation requirements has been criticized in the popular press.

Figure 1 shows a schematic of a high-bypass fan jet engine bleed air system which is typical for commercial airliners [12]. Hot compressed air is taken from the engine compressor and cooled in the pre-cooler to temperatures around 175^{o}C before being supplied to the environmental control system and other functions on the aircraft. Modern engines have two bleed air ports at different stages of the compressor in order to minimize excess temperature and pressure in the bleed air and to maximize engine energy efficiency. The actual temperature and pressure of the air exiting the engine compressor can be as high as 350^{o}C and 1.2 MPa or as low as 185^{o}C and 0.21 MPa depending upon the phase of flight and engine operation [1]. If the aircraft is equipped with an ozone converter, the converter is normally located downstream of the pre-cooler but before the air is further cooled to cabin temperatures since most ozone converters work best at elevated temperatures. The pre-cooler is a cross-flow, air-to-air heat exchanger located in the engine pylon just aft of the fan and immediately above the engine compressor as shown in Figure 2 [13]. The pre-cooler uses ducted fan air to cool the hot bleed air from the compressor. The bleed air lines from the engine to the pre-cooler are not long so that the exposure times to the highest temperatures could be very brief. Chemical reaction kinetics are expected to play an important role in the reactions that occur with the contaminants in the bleed air. Most of the important chemical reactions associated with decomposition and possible pyrolysis of bleed air contaminants occur either within the engine compressor itself or in the hot section of the bleed air path between the compressor and pre-cooler.

The air from the bleed air system shown in Figure 1 is directed to the cabin through air-conditioning packs where the air is further cooled in air cycle machines. The air from the air-conditioning packs is then directed to the mixing manifold where it is mixed with cabin recirculation air for distribution throughout the aircraft.

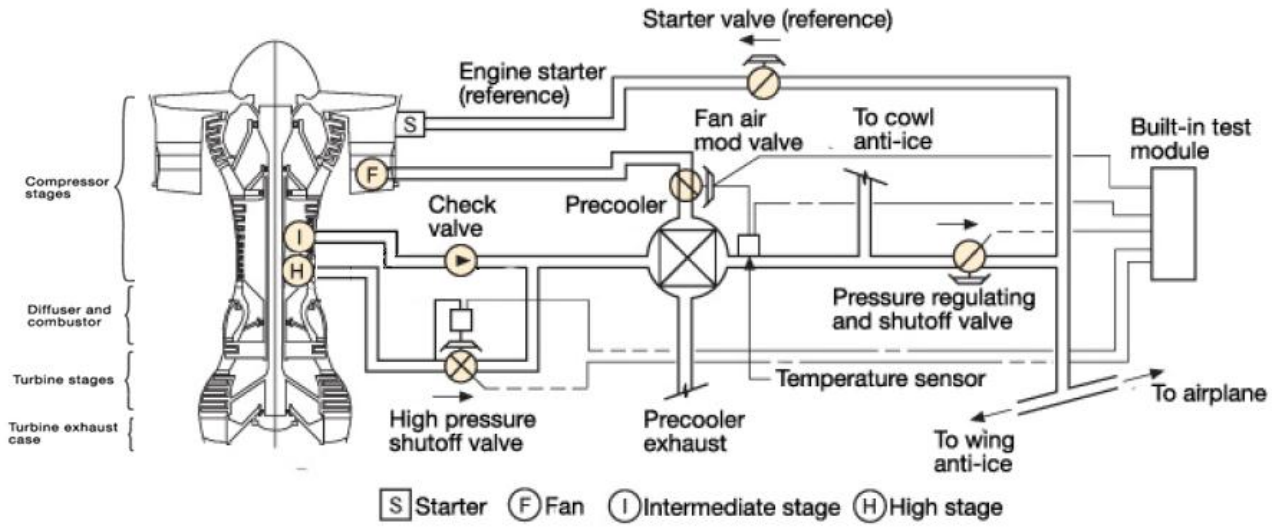

Figure 1. Typical Airliner Bleed Air Supply System adapted from [12].

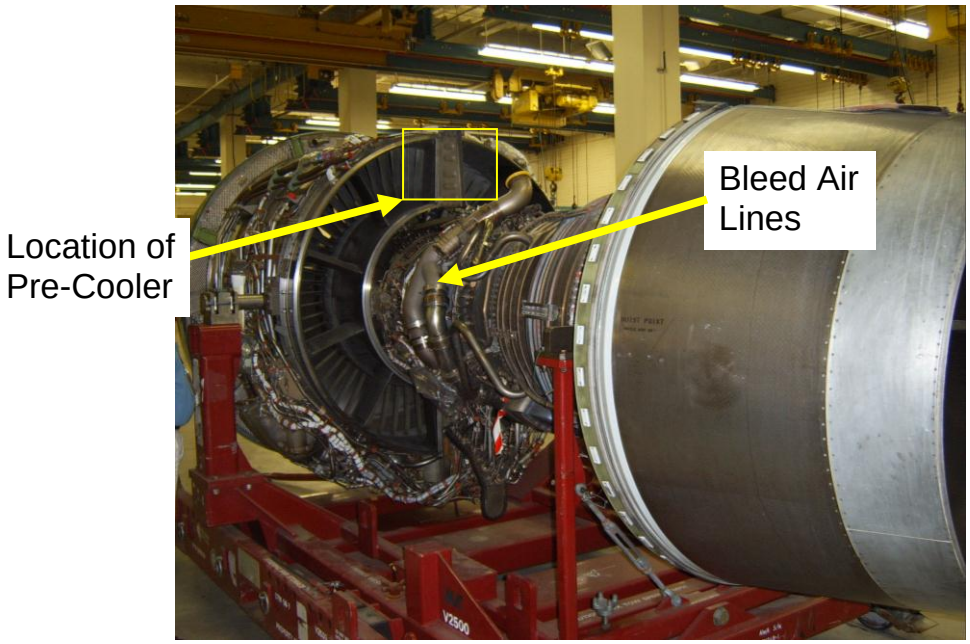

Figure 2. Modern aircraft turbofan jet engine: location of the compressor bleed air lines and the bleed air pre-cooler [13].

2.2 Thermal Degradation of Aircraft Working Fluids

Van Netten *et al.* [14-16] evaluated the thermal degradation of a number of hydraulic fluids and jet engine oils during heating on a ceramic hot plate. A thermocouple was used to monitor the temperature of the hot plate. Gases were evolved into a 250 L stainless steel chamber equipped

with a multigas monitor TMX-412 (Industrial Scientific Corporation, Oakdale, PA) to measure NO_2, oxygen (O_2), and carbon monoxide (CO). Additionally, a YES-204A monitor (Young Environmental Systems, Richmond, B.C., Canada) was also located in the chamber to measure temperature, relative humidity, and carbon dioxide (CO_2) concentration [16]. Samples were heated to 525°C at a rate of 10°C/min and were then held at 525°C for 1 minute before cooling to room temperature. Monitoring of the ambient air began before the oil was inserted into the test chamber. Air samples were also retrieved from the chamber for subsequent analysis by gas chromatography/mass spectrometry (GC/MS).

Van Netten *et al.* [14] noted that Mobil Jet Oil 254 (Exxon Mobile Corp., Fairfax, VA) was initially dark blue in color at room temperature. White smoke began to form when the hot plate reached approximately 275°C and the oil turned a dark brown-orange color. Charring of the oil began at 400°C while white smoke continued to form. At 500°C, only some charred material remained on the oil sample holder. Gas concentrations of 102.5 ppm CO and 460 ppm CO_2 were detected at 525°C [13]. Air sample results from GC/MS analysis indicated the presence of TCP isomers as well as volatile derivatives of pentane, hexane, and octane during degradation of Mobil 254 jet engine oil.

Castrol 5000 jet engine oil (BP North America, Parsippany, NJ) was initially orange in color and this lubricant began producing white smoke at approximately 285°C. Darkening of the oil began at 310°C, charring was observed at 350°C and only charred brown material remained at the end of thermal degradation. The CO_2 sensor measured a peak of 510 ppm CO_2 while the CO sensor detected a maximum of 140 ppm CO during degradation of the Castrol 5000 [16].

Van Netten *et al* [14] noted that Exxon Turbo Oil 2380 (Exxon Mobile Corp., Fairfax, VA) began producing white smoke at about 275°C and darkening of the lubricant began at 300°C. Charring was observed at 310°C. At the end of the experiment only charred brown material remained. The CO_2 sensor measured a peak of about 510 ppm CO_2 and the CO sensor measured a peak of approximately 120 ppm CO [16].

Crane *et al* [17] also evaluated Exxon Turbo Oil 2380. These researchers utilized a custom-built combustion chamber to degrade the samples and analyze the evolved gas samples. The total volume of this chamber was only 12.6 L. Three milliliters of sample were placed in a semi-cylindrical quartz combustion boat located in a horizontal quartz tube furnace. The sample was continuously heated from room temperature until only charred material remained. Exxon 2380 began producing a measurable amount of CO at around 306°C when the authors also noted an increase in visible smoke production. At 344°C, the CO concentration was measured as 5,000 ppm. Only charred material remained when the temperature reached 350°C. The residual solid char continued to produce CO up to 530°C. Crane *et al* found that as the thermal decomposition temperature increased, the production of CO began earlier and the maximum measured values of CO in the chamber increased. When Exxon Turbo Oil 2380 was thermally degraded at 600°C, the authors reported a much higher CO level of 17,000 ppm CO.

Bartl *et al* [18] evaluated thermal degradation of pentaerythritol derivatives (the base component of jet engine oils) using thermogravimetric analysis (TGA) and differential thermal analysis

(DTA). These researchers heated 10 mg of pentaerythritol from room temperature to 1000°C at 10°C/min in air. Figure 3 shows typical TGA and DTA data. The sample began to lose weight at approximately 275°C (which is roughly the temperature van Netten *et a*l [14] began seeing visible smoke generation). The DTA data indicates sample heating due to exothermic reactions (i.e., burning) in the oil as the oil degrades. The first peak at approximately 350°C corresponds to a lower temperature oxidation reaction in which low molecular weight hydrocarbons were produced. The second higher temperature peak at about 570°C was likely due to oxidation of any remaining oil and charred products to CO and CO_2. This can be roughly associated with the smoke, CO and CO_2 evolution at 525°C reported by van Netten *et al*[14].

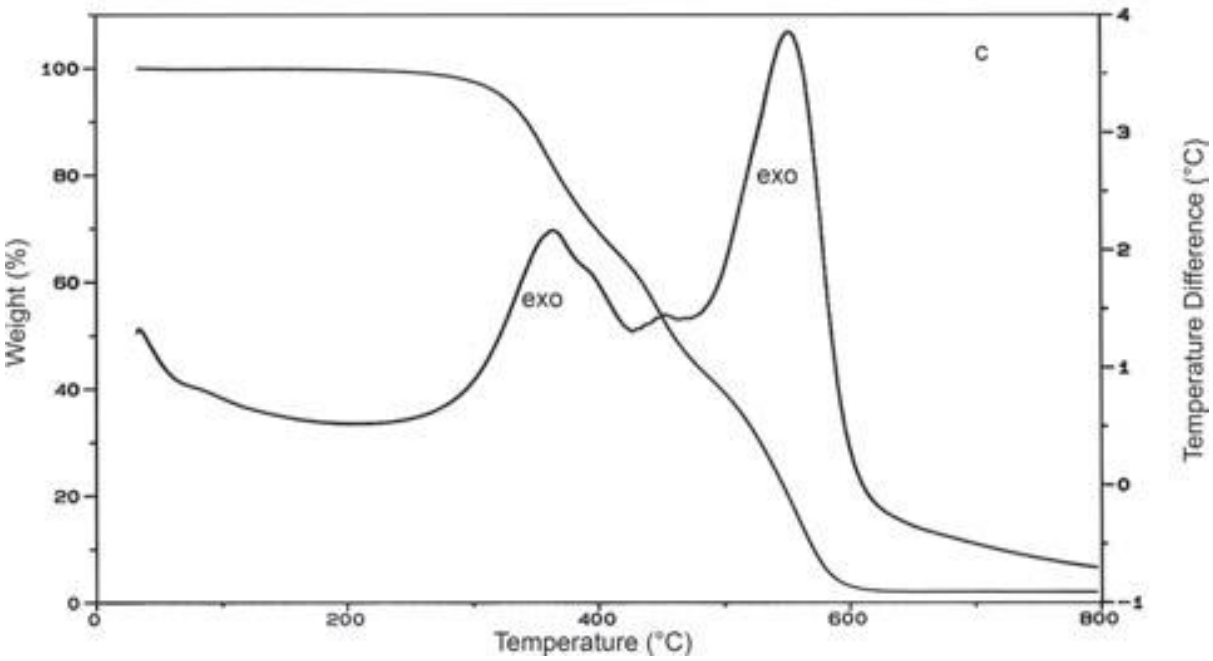

Figure 3. TGA and DTA plots of pentaerythritol derivative in air [17]. The low temperature exothermic peak at about 350°C corresponds to low temperature oxidation producing smoke, low molecular weight hydrocarbons, CO and CO_2. The higher temperature exothermic peak corresponds to oxidation of the remaining oil and charred oil to smoke, CO and CO_2.

2.3 Summary of Gaseous Contaminant Targets for Detection

Although Ref.[1] notes a wide range of gaseous contaminants of potential concern in aircraft including human bioeffluents (e.g., ethanol, acetone), cosmetics and perfumes (e.g., benzene, limonene, toluene, xylene, etc.) and dry cleaning agents (e.g., tetrachloroethene), the focus of this work is on those air contaminants that might arise from inadvertent malfunctions connected with

the bleed air supplies from either the aircraft engine or the auxiliary power unit (APU). As noted in Section 2.2 and summarized in Table II below, the principal contaminants of the aircraft bleed air supply could include (1) aerosolized droplets of jet engine or APU lubricating oil and (2) partially or fully pyrolized by-products of combustion of the working fluids. A number of approaches exist for monitoring of environmental air quality on aircraft to detect contamination of the bleed air supplies. Sensors could be located in either (i) the passenger cabin, (ii) along the bleed air supply path between the pre-cooler and the air conditioning packs, or (iii) between the air conditioning packs cooling the bleed air and the mixing chamber where the bleed air is mixed with the cabin recirculation air. The following section reviews the abilities of commercially available sensor technologies to detect these potential air contaminants.

Table II
Summary of Potential Bleed Air Contaminants

Potential Bleed Air Contamination Event	*Probable Contaminant*
Engine oil leak producing aerosolized droplets of oil in the engine compressor	• Very fine mist of engine oil aerosols • Small amounts of carbon monoxide (CO) and carbon dioxide (CO_2)
Partially pyrolized jet engine oil	• Very fine mist of engine oil aerosols • Carbon monoxide (CO) • Carbon dioxide (CO_2) • Misc. unburned hydrocarbons • Ultrafine smoke particles
Fully pyrolized jet engine oil	• Carbon monoxide (CO) • Carbon dioxide (CO_2) • Ultrafine smoke particles

2.4 Review of Commercial Gas Sensing Technologies

A rapidly increasing body of literature exists concerning environmental gas sensors that generate electrical signals (i.e., voltages or currents) in response to the presence of a contaminating analyte in air. Typical contaminants of interest include CO_2 in the air supplies of office buildings, CO from the exhaust of combustion processes in garages and other enclosed spaces and a wide variety of process gases in numerous industrial applications. Scientists and engineers worldwide are searching for ways to improve the intrinsic responses of the basic sensing materials. However, commercial sensor systems contain not only the discrete sensor element itself, but also the various technologies needed to transport the gaseous contaminant to the sensing material as well as the required electronics needed to supply power plus acquire, condition and transmit the

sensor signals. A brief review is presented below for commercially available air quality sensors that might be applicable to aircraft air quality sensing. This review does not include either very advanced sensing technologies that have yet to demonstrate significant market acceptance (and corresponding user experience) or expensive and labor intensive laboratory-class sensing techniques that would not likely find acceptance for routine operation within the aviation community.

Catalytic-bead sensors have been used commercially for many years to detect the presence of combustible gases. Early devices used a heated platinum wire to initiate combustion of the gas to be detected. The sensor electronics compared the resulting resistivity increase in the sensing platinum wire (due to increased temperature from combustion) to a reference wire that had been treated to prevent combustion. The sensor wire and the reference wire were connected in a Wheatstone bridge circuit to facilitate comparison. Sensor response to the target gas is enhanced in modern designs that utilize specially formulated catalyst containing porous beads around the heated platinum wires [19]. A schematic of a catalytic bead sensor is shown in Figure 4(a). Unfortunately, high operating temperatures are required for catalytic sensors and the devices are not particularly selective in their response to various combustible gases [20].

Metal-oxide semiconductor (MOS) sensors rely upon ionic absorption of the analyte's gaseous molecules to induce either a current or a voltage in the sensor material. See Figure 4(b). Two fundamental types of metal-oxide conductivity sensors exist: (1) n-type (e.g., tin oxide or zinc oxide) that, after reaching equilibrium with the oxygen in the air, react with reducing gases like CO to release electrons and increase the conductivity of the oxide and (2) p-type (e.g., nickel oxide or cobalt oxide) that react with oxidizing gases like O_2 , NO_2 or O_3 to consume electrons -- producing holes (i.e., charge carriers) and also increase the conductivity of the oxide [22]. Selectivity of the sensor to specific gases of interest can be improved by careful selection of the sensor alloy dopant, the operating temperature of the sensor material and gas filtration techniques [22]. Unfortunately, like catalytic bead sensors, high operating temperatures are also required for solid-state sensors.

Electrochemical sensors can be designed as either current generating (amperometric) or voltage generating (potentiometric) in response to the presence of the gas constituent to be measured [23-25]. In the case of a potentiometric sensor, the gas of interest establishes an electrochemical potential, which generates an open circuit voltage relative to a reference electrode. In the case of an amperometric sensor, as shown in Figure 4(c), a reducing (or oxidizing) gas of interest is oxidized (or reduced) at the working electrode. The magnitude of the current generated by this oxidation (or reduction) reaction is related to the concentration of the gas of interest. Solid polymer electrolytes emerged in the middle 1970s to alleviate some of the maintenance issues associated with aqueous electrolyte solutions [23]. In addition, ceramic oxide electrolytes are being investigated for monitoring the gaseous by-products of combustion [24,25].

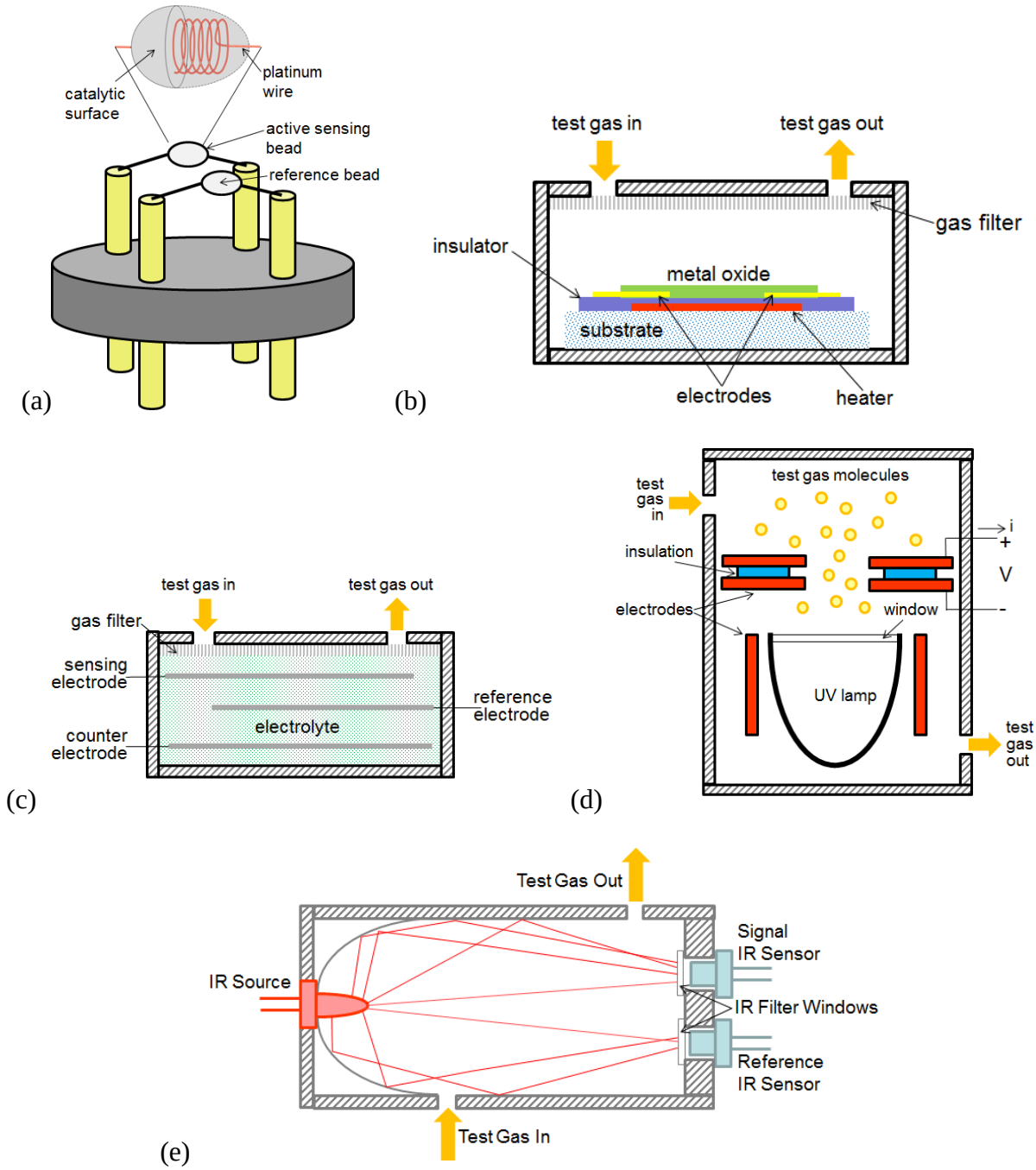

Figure 4. Schematic representation of commercial gas sensor detection technologies.
(a) catalytic bead sensors typically used to detect inflammable gases;
(b) conductometric sensors based upon metal-oxide semiconductor materials;
(c) 3-electrode configuration of electrochemical sensors;
(d) schematic representation of photoionization detectors for detecting volatile organic compounds like benzene, ethanol, acetone, amines and ammonia; and
(e) two channel non-dispersive infra-red (NDIR) sensor often used for measuring CO2 in HVAC systems.
Schematics (a) and (d) adapted from [21]

As shown in Figure 4(d), *photoionization detectors* (PIDs) use light from an ultraviolet (UV) lamp to ionize gas molecules with ionization potentials less than the UV energy produced by the lamp [26]. Detector electrodes in PIDs are biased with a DC voltage and collect the free electrons from the ionized molecules. Detector current flows are thus proportional to the amount of the ionizing species. Many photoionization detector lamps use krypton gas in the UV lamp. Such lamps emit UV energy at 10.6 eV and can detect VOCs such as benzene, ethanol, acetone, amines, ammonia and aromatic compounds. The principal disadvantage of photoionization detectors resides in the requirement that the sensor window be kept clean to ensure consistent performance.

Dedicated *infrared sensors* often use simple heated filaments to emit broadband IR radiation through the gas mixture of interest [21]. The radiation is then filtered to a narrow bandwidth IR beam for measurement by an IR sensor. Figure 4(e) shows one configuration that uses a single lamp, dual wavelength design where the second wavelength/detector combination monitors a wavelength expected to exhibit no absorption in air. This measurement is thus independent of the gas mixture and provides a reference signal for sensor compensation due to variations in lamp intensity and light scattering from particulates. The narrowly filtered bandwidth of these non-dispersive infrared (NDIR) sensors does not create complete spectral fingerprints of gases but instead enables measurement of the absorption of the narrow beam at a specific wavelength. According to Beers law, the amount of IR absorbed is proportional to the amount of the gas species in the detection pathlength. The actual wavelength can be selected and tuned to a specific and well-behaved IR absorption peak for a specific gas of interest. The principal disadvantages of NDIR sensors are in the sensitivity of the optical components to impact and vibration as well as maintenance of the cleanliness of the sensor windows for reliable operation.

NDIR sensors are finding increasing utilization in building HVAC systems to monitor levels of CO_2 in indoor air and modulate the intake of fresh outdoor air. This application is often referred to as Demand Controlled Ventilation and enables building owners to reduce the energy costs associated with over ventilating buildings during times of low occupancy. Commercial CO_2 sensors are available from a number of companies and Shrestha and Maxwell [27-30] investigated the abilities of commercial NDIR sensor systems to accurately and consistently evaluate the level of CO_2 under a range of environmental conditions including humidity, temperature and pressure. These researchers found wide performance variations among sensors of different manufacturers and sometimes even between identical sensor systems from the same manufacturer. Of particular concern was the automatic baseline adjustment algorithms incorporated in some sensor systems. This algorithm could introduce bias into the readings as the sensor systems attempts to automatically correct sensor readings to the expected value of 400 ppm CO_2 during the overnight periods of building vacancy. Shrestha and Maxwell note that NDIR CO_2 sensor systems should be individually calibrated prior to being placed into service. Periodic recalibrations would then appear to be warranted.

Table III summarizes the possible bleed air contaminants and the commercial sensor technology typically applied to detect and monitor the various contaminants in various non-aerospace applications.

Table III
Possible Bleed Air Contaminants and Potential Sensor Technologies

Possible Bleed Air Contaminant	*Commercial Sensor Technology*
• Engine oil aerosols • Ultra-fine smoke particles	• Light scattering photoelectric detectors (dia>0.5 μm) or ionization detectors (dia<0.5 μm) depending upon the aerosol/particle size distribution
• Carbon Monoxide (CO)	• Electrochemical cell sensor with selectivity optimized for CO
• Carbon Dioxide (CO_2)	• Non-dispersive Infrared (NDIR) sensor optimized for CO_2)
• Misc. unburned hydrocarbons	• Catalytic bead sensor OR photoionization detector depending upon the specific hydrocarbon(s) to be detected

3.0 Methods and Materials

3.1 Evolved Gas Analysis by TGA/FTIR/MS

The Thermoanalytical Section of the NETZSCH Instruments Applications Laboratory (Burlington, MA) examined four common jet engine oil samples supplied by Auburn University. The temperature-dependent mass changes and evolved gases were analyzed using the NETZSCH TG 209 ***F1*** *Iris*® thermogravimetric analyzer (TGA) coupled to a BRUKER Optics FTIR *TENSOR*™ and a NETZSCH QMS 403 *Aeolos* mass spectrometer [31]. A schematic of the experimental system is shown in Figure 5. The NETZSCH TG209**F1** *Iris*® instrument can measure mass changes from 20°C to 1000°C with a resolution of 0.1µg. The heating rate is variable from 0.1 K/min and 100 K/min. The evolved gases were analyzed with a NETZSCH QMS 403 *Aeolos* system simultaneously coupled to the NETZSCH TG209**F1** *Iris*® by means of a transfer line which was kept at a constant temperature of 250°C. The mass spectrometer of the QMS 403 allows detection of mass numbers between 1 and 300 amu. The evolved gas analysis was performed using the combined TGA-MS MSÒ-Windows analysis software package.

The oil samples and masses investigated were: BP Turbo Oil 274 (5.46 mg), BP Turbo Oil 2380 (5.01 mg), Aeroshell Turbine Oil 560 (5.65 mg) and Mobil Jet Oil II (5.22 mg). The samples were heated in platinum crucibles in air from room temperature to 650°C at 10°C/min.

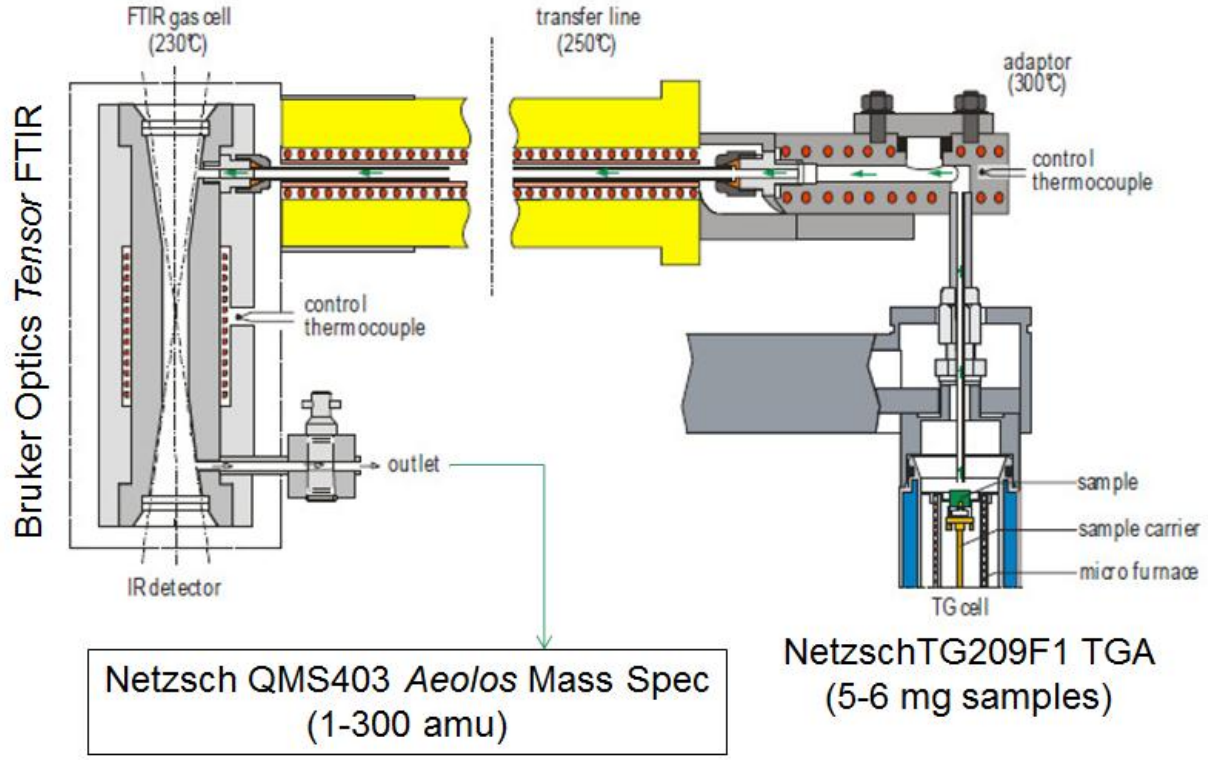

Figure 5. Evolved gas analysis experimental arrangement used by NETZSCH Instruments Applications Laboratory.

3.2 Sensor Evaluation Procedures

3.2.1 Variable Pressure Commercial Sensor Test System

The experimental setup utilized to evaluate commercial CO and CO_2 sensors consisted of four major modules as illustrated in Figure 6.

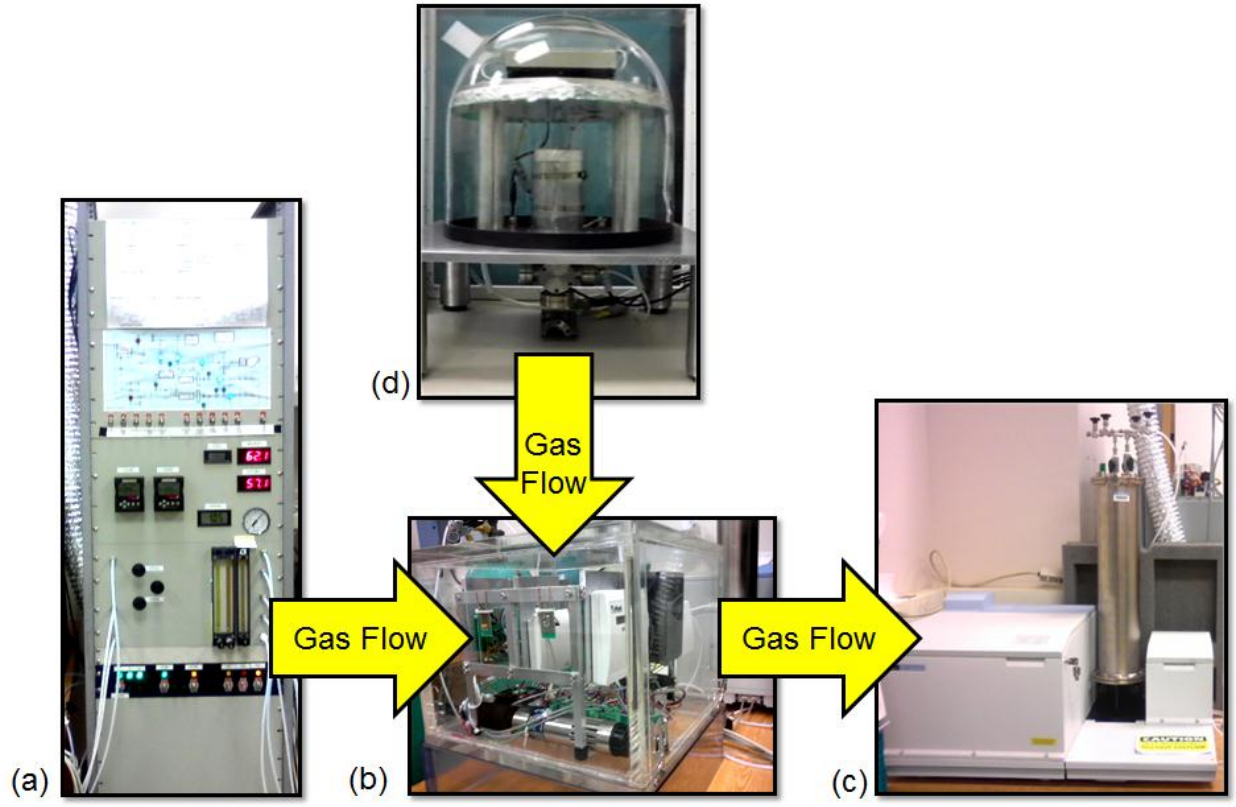

Figure 6. Experimental arrangement for testing commercial CO and CO_2 sensors.

The Calibration Gas Control Module is shown in Figure 6(a) and is responsible for the control of pressure, flow rates and mixing of inert carrying gases (typically nitrogen or nitrogen with 20% oxygen) as well as the contaminant test gases of interest (e.g., CO, CO_2). The pressure setting within the system allows for testing of sensors at pressures representative of altitudes that are encountered in the airplane cabin environment. The gas lines in the system are rated for vacuum pressures of 15 inches of mercury (380 mm Hg) or about 50% of atmospheric pressure (50.5 kPa), which corresponds to altitudes up to 12,000 feet (3,700 meters). The flow meters allow precise control of the gases and allow custom mixing ratios for sensor performance testing.

The Commercial Sensor Analysis Module shown in Figure 6(b) is an enclosed, vacuum-sealed, PMMA chamber, which has a total volume of 42.4 liters. With this module, an environment replicating the low pressure airplane cabin can be maintained to test commercial sensor performance in regards to detection of the gases of interest.

The Oil Degradation Module, shown in Figure 6(d), includes a microbalance from which 1g oil samples were suspended into a cylindrical heater. The Scientech SM124D (Boulder, CO) microbalance measured the mass of the sample within ±0.6 mg over the experimental mass range. The temperature of the oil sample was measured within ±2˚C over the experimental temperature range (room temperature to 600˚C). The Watlow ceramic fiber heater (Chicago, IL) has a operating range up to 2200˚C. The microbalance-heater assembly was encapsulated by a 50 L bell jar to contain the evolved gases. Room temperature air from outside the bell jar was provided within the upper region of the bell jar (adjacent to the microbalance) by two plastic tubes, approximately 12 mm in diameter. The supply outside air was forced through a 12 mm hole below the balance and down through the heater past the hanging crucible assembly. In addition, a vacuum pump connected to the FTIR pulled the air from the bell jar, at a rate of 11,600 sccm via a tube that connects both the sensor chamber and the FTIR to the thermal degradation system. See Figure 6(c). This prevented any evolved gases from migrating into the top of the bell jar and affecting the performance of the microbalance. The thermal degradation system was enclosed by a custom built fume hood to contain any possible leaks in the system. Once the evolved gases passed through the sensor chamber and the FTIR, they were removed by the building exhaust.

The FTIR Gas Analysis Module shown in Figure 6(c) was used as the standard to verify the gas composition of various concentrations of test gases used for evaluating sensor performance. This module contained a Spectrum GX FTIR System (Perkin Elmer, Shelton, CT, USA), as well as an M-5-22-V variable pathlength long-path gas cell (Infrared Analysis, Inc., Anaheim, CA, USA). The optical path is folded in a total volume of 8.5 liters, while the cell path length was held constant at 2.24 m. The analyzed wavenumber range has typically varied from 600 cm^{-1} to 4000 cm^{-1} with a spectral resolution of 0.5 cm^{-1}. The IR source was produced by a temperature stabilized wire coil that operates at 1350 K. The material for the cell windows in the variable pathlength long pass gas cell are potassium chloride (KCl) and are 4 mm thick. The detector for the IR beam is a fast recovery deuterated triglycine sulfate (FR-DTGC) module.

3.2.2 Tricresyl Phosphate Sensor Development and Testing

TCP samples were converted by alkaline hydrolysis to cresol which enables application of standard electrochemical detection techniques. A schematic of the process is shown in Figure 7(a, b).

Reagents and alkaline catalyst for TCP hydrolysis: Alkaline powder catalyst was prepared by mixing sodium hydroxide and alumina (1:10 wt) in ethanol while stirring for 1h until all sodium hydroxide was dissolved. The mixture was then dried in a vacuum chamber and the dried powder heated to 100^{o}C before use. 100 mg of powder was packed into a 20 µL beveled pipette filter tip to form the hydrolyzing column.

P-cresol (Acros Organics, NJ, 99+%) was dissolved in 0.2 M Na_2HPO_4/0.2 M KH_2PO_4 buffer (pH = 6.67, NaCl = 10 mM) to establish a sensor calibration standard. Deionized water used was obtained from a Millipore Direct-Q water purification system (resistivity 18 $M\Omega cm^{-2}$).

Electrodes and Sensor: All amperometric experiments were performed with CH Instruments (CH1910B) Bi-Potentiopstat and duplicated with a handheld potentiostat (Palm-Sens). A desktop computer and pocket PC were used to collect the respective data. The handheld potentiostat communicated wirelessly with the Pocket PC via Bluetooth®. Flow injection analysis (FIA) was carried out using cell electrodes, one of which includes a glassy carbon working electrode (2 mm dia.), and another of which includes a stainless steel auxiliary electrode and Ag/AgCl reference electrode (BASi, IN). A coating solution was applied to the Ag/AgCl reference electrode before detection as per instructions from the manufacturer. The working electrode was polished with alumina powder (1, 0.3, and 0.05 μm in order). 10 mM NaCl was used to maintain the potential of the reference electrode. A switch injection unit (Valco Instruments Co. Inc) was used with a 50 μL sample loading loop. The flow rate was maintained at 200 μL/min by using a single syringe pump (KD Scientific, MA).

TCP sampling from methanol solutions or oil samples: Since TCP samples in a gas phase are not readily available, it was necessary to prepare such samples for the system calibration. The stock TCP solution (0.002 M) was prepared in methanol and diluted to obtain TCP samples with concentrations of interest. 0.4 mL of each TCP sample solution was then gasified by 5 min of N_2 (gas) blowing, followed by 5 min of N_2 blowing concurrent with 220^{o}C heating in a silicon oil bath. See Figure 7(a). The flow rate of N_2 was maintained at 1.1 L/min. Because of the low saturated vapor pressure of TCP at room temperature (less than 10^{-7} atm), heating was necessary to completely gasify the TCP to be blown through the alkaline catalyst column and converted to cresol.

Engine oil samples were prepared by dissolving the samples into methanol. The oil samples were sampled with the same processes as the TCP the samples. BP274 jet engine oil does not contain TCP while BP2380 includes 1-5% TCP [16].

After collecting each gas sample for 10 min, the catalyst column was flushed with 3 mL of phosphate buffer (0.2 M Na_2HPO_4/0.2 M KH_2PO_4) as shown schematically in Figure 7(b). 0.01M NaCl was added into the buffer to maintain the potential of the reference electrode. The converted TCP samples were then injected into the buffer solution and the cresol was detected by electrochemical sensors as shown in Figure 7(c). The TCP sampling process was performed automatically utilizing electronic relays, valves, pumps, and tubes.

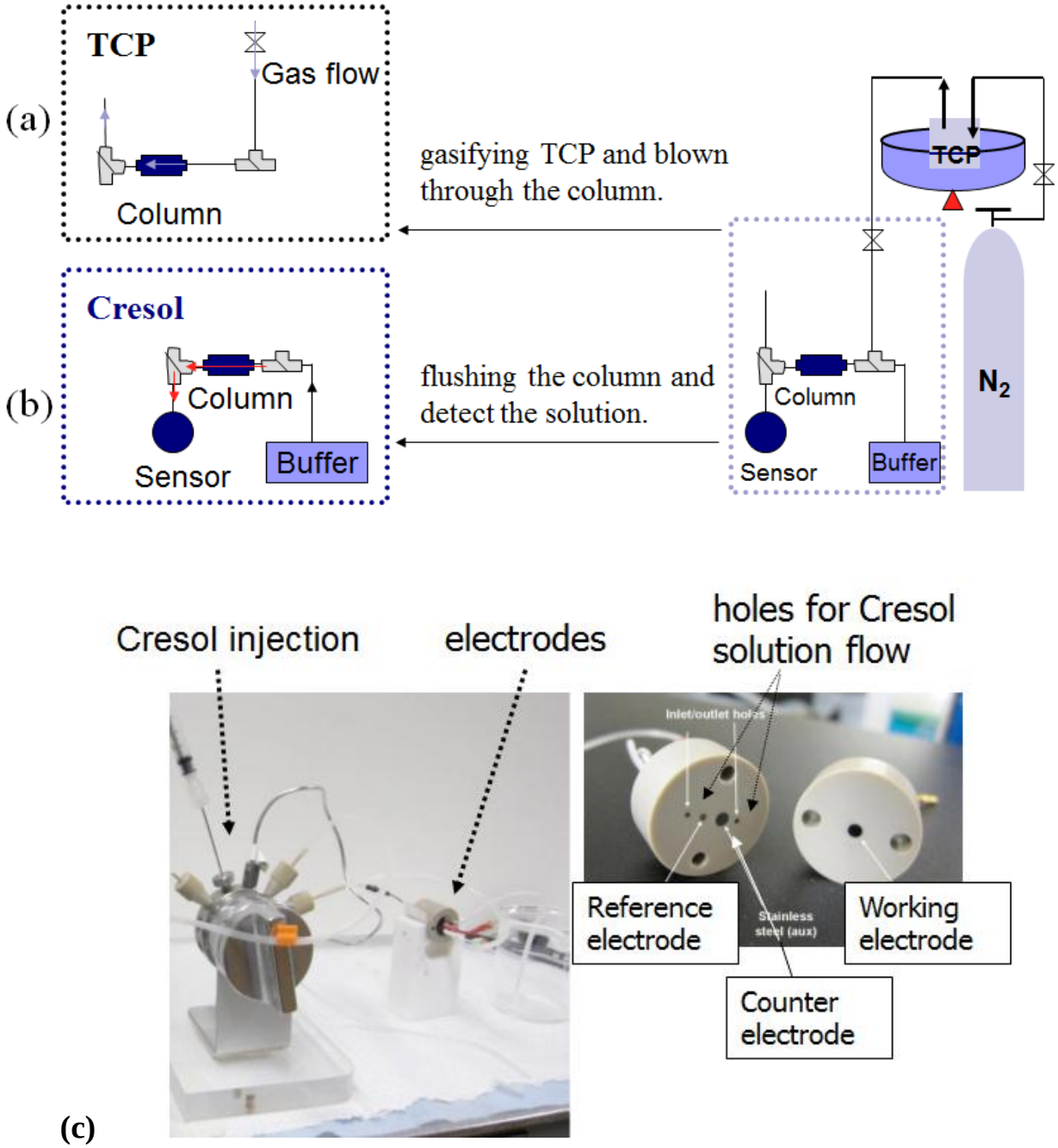

Figure 7. Tricresyl phosphate sensor development system; (a) Schematic of the TCP/methanol solution gasification and hydrolysis into cresol. (b) Schematic of the buffer washing of the cresol from the alkaline catalyst and injection into the electrochemical detector. (c) Flow injection system and flow cell electrodes were used to detect samples containing cresol.

3.3 Data Mining of the FAA SDRS and NASA ASRS Databases

The FAA Service Difficulty Reporting System (SDRS) database provide a web application front-end that allows users to query the underlying database. However, the provided web application interface was too cumbersome for quickly and easily running (i) multiple queries and/or (ii) complex queries. Thus it was decided to download the entirety of the database and create a local copy that could be quickly and easily mined for associations. With privileged access to the SDRS data, the entirety of the database was then downloaded in the form of multiple, tab-separated value files. A local copy of the database enabled many queries to be processed without using excessive Internet bandwidth or potentially tying up the database server with our large queries. Another benefit of having a local copy of the data was that complex queries were possible that were not limited to solely what the web application interface allowed. A script was written to parse the data from the files, eliminate errors associated with the transfer, and then store the data into an SQLite database. SQLite was chosen because it is very easy to use, is reasonably fast, and creates a single database file that can be easily shared.

The data in the NASA ASRS (Aviation Safety Reporting System) database was all collected via the available public web application interface, but was downloaded and parsed in a similar manner to the FAA SDRS database.

3.4 Wireless Sensor Network Field Test in an Aircraft Cabin Mock-up

On August 2nd 2011, Boise State University deployed a custom wireless sensor network within Kansas State University's Boeing 767 mock-up cabin section to verify the feasibility of capturing measurements of highly dynamic environmental conditions present in aircraft bleed air systems and airliner cabins. The sensor network consisted of 12 wireless sensor units and a base station. Each wireless sensor unit was configured to measure four environmental conditions: CO_2, temperature, humidity, and atmospheric pressure. The 12 sensor units were uniformly distributed across the cabin such that each seating section had sensor modules located at 100" intervals down the length of the cabin. This configuration resulted in a 76" spacing laterally between modules. The modules were placed on the top of the seatbacks to provide proximity to seated passenger head level. Figure 8 shows a diagram of the sensor module locations within the cabin section.

Two test series were performed. The first test series (Series 1) primarily tested humidity dispersion and provided a basic test of the system. During Series 1, humidifiers were located in two different areas within the cabin (P1 and P2 in Figure 8). The other three environmental parameters (CO_2, temperature, and pressure) were also acquired during the humidity testing. The second test series (Series 2) primarily tested CO_2 dispersion through the cabin. Unlike the humidity sources used in Series 1, the CO_2 injection point remained fixed across all test runs as the CO_2 injection point was not adjustable in the cabin system.

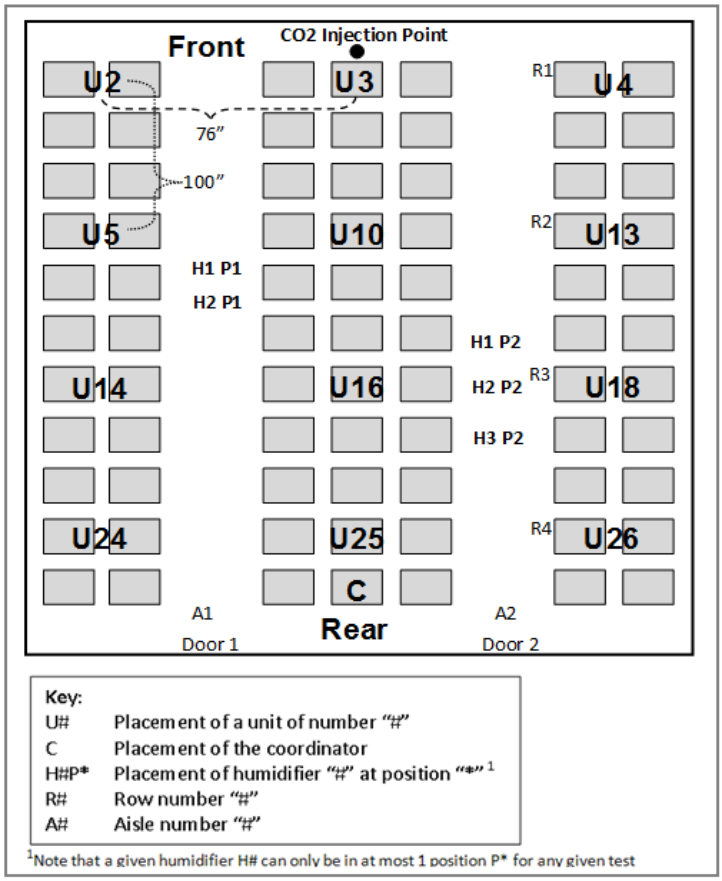

Figure 8. Kansas State University's B767 Cabin Layout and Sensor Network Test Configuration

4.0 Results and Discussion

4.1 Characterization of Fumes from Oil Degradation Experiments

Figure 9 shows the change in sample mass as a percentage of the total (TG) and the mass change rate (DTG) as the sample heated from room temperature to 650°C. In addition the Gram-Schmidt reduced data set shows essentially the total integrated intensity of the FTIR spectra and peaks or shoulders in the Gram Schmidt curve can be interpreted as the appearance of new species in the evolved gas mixture. The TG data show mass loss beginning at around 200°C with the rate of maximum mass loss occurring at 300.2°C (DTG). The peak in gas evolution is shown to occur at 300.8°C in the Gram Schmidt data in close agreement with the sample mass loss data.

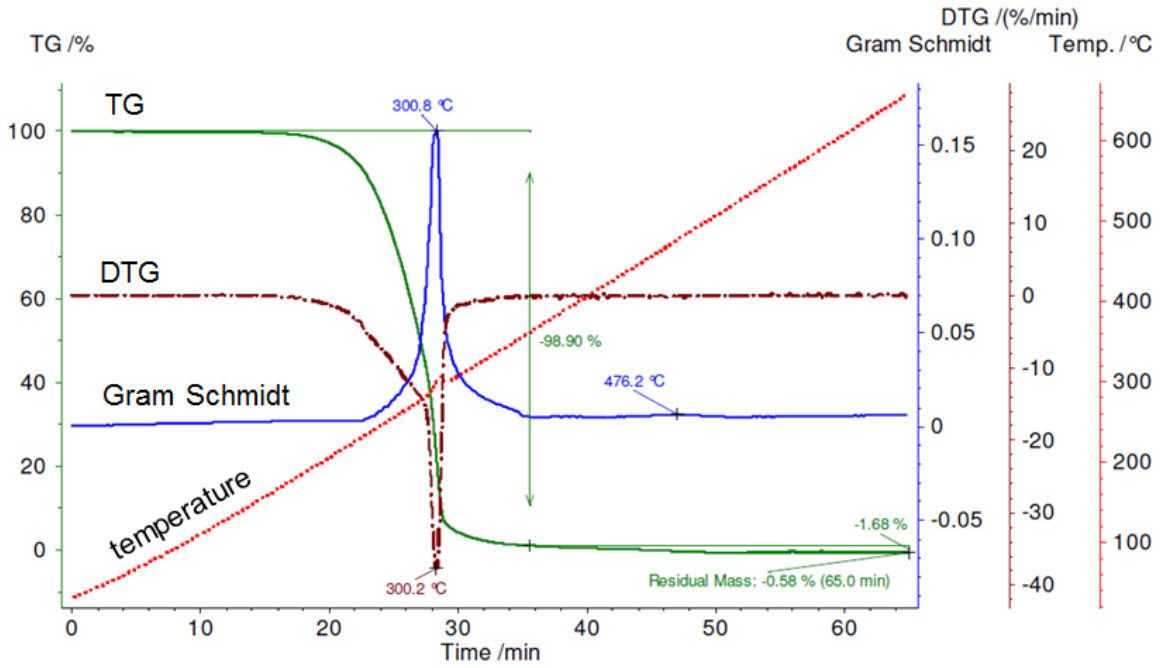

Figure 9. Mass changes of BP274 oil sample as a function of exposure temperature. Sample size = 5.46 mg and 10°C/min heating rate in air. (TG=mass change, DTG=mass change rate)

The BP Turbo Oil 274 mass spectrometry ion-current curves for H_2 (2 amu), H_2O (17; 18 amu) and CO_2 (12; 44 amu) are plotted in Figure 10(a) along with the already analyzed TG data. All the species evolve as a sharp peak at 293.5°C. Figure 10(b) shows the mass spectrometry ion-current curves for C_2H_5 (29 amu), C_2H_6 (30 amu), CH_2OH (31 amu), CH_3OH (32 amu), H_2S (34 amu), C_3H_3 (39 amu) and C_3H_7 (43 amu) along with the already analyzed TG data. C_2H_6, C_3H_3 and C_3H_7 evolve as a sharp peak at 293.5°C, while the signals for all the other fragments and molecules show a broad asymmetric peak.

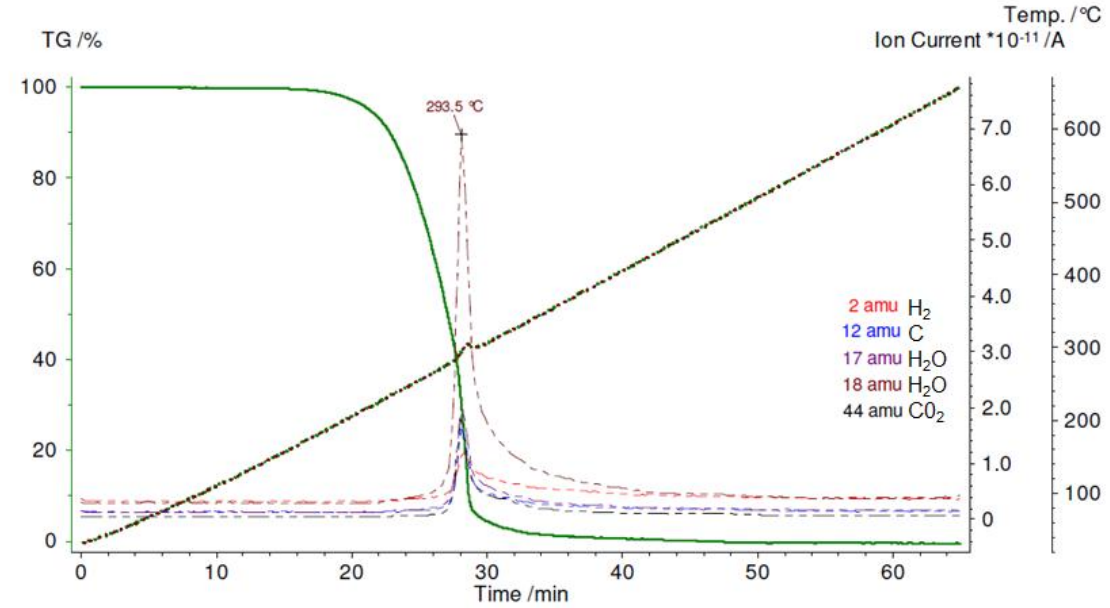

(a)

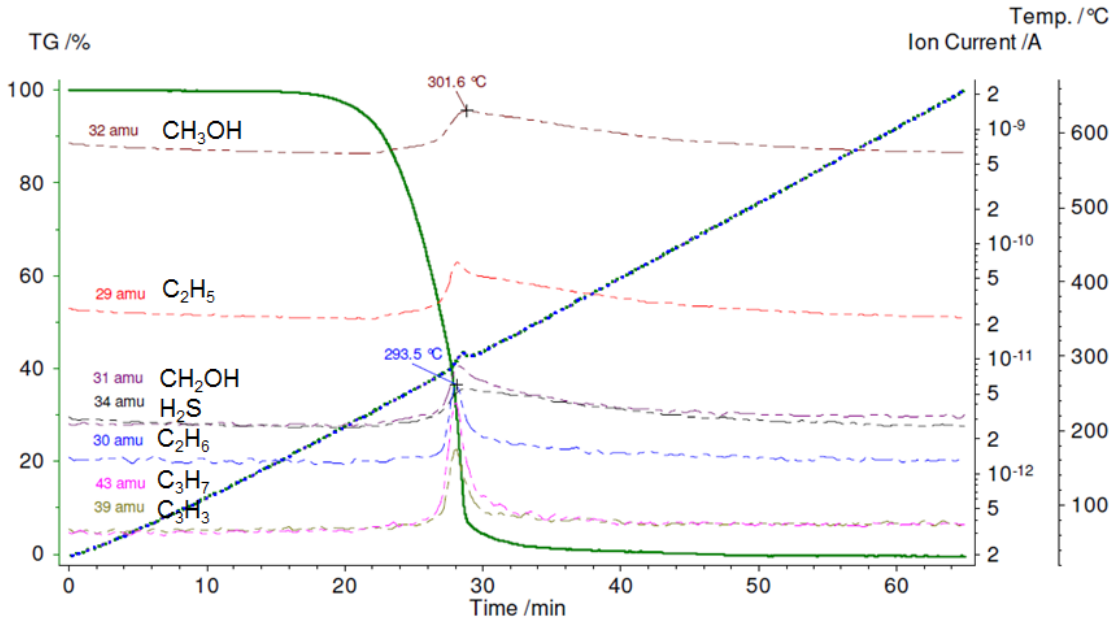

(b)

Figure 10. Time dependent mass loss and sample temperature data shown with mass spectrometry ion-currents for the following evolved gaseous species: (a) 2 amu – H_2, 12 amu - C, 17 and 18 amu – H_2O, 44 amu – CO_2; (b) 32 amu – CH_3OH, 29 amu – C_2H_5, 31 amu – CH_2OH, 34 amu – H_2S, 30 amu – C_2H_6, 43 amu – C_3H_7, and 39 amu – C_3H_3.

Additional experiments with BP Turbo Oil 2380, Aeroshell Turbine Oil 560 and Mobil Jet Oil II yielded similar results for peak degradation temperatures and evolved gases. The peak degradation temperatures are summarized in Table IV and show that all the oils exhibited the greatest mass losses at temperatures ranging from 301-325 ^{o}C.

Table IV
Jet Engine Oils: Peak Degradation Temperatures

Jet Engine Oil	*Peak Degradation Temperature*
BP Turbo Oil 274	301 ^{o}C
BP Turbo Oil 2380	305 ^{o}C
Aeroshell Turbine Oil 560	326 ^{o}C
Mobil Jet Oil II	307 ^{o}C

A 3-D plot of FTIR spectra vs. time for the BP Turbo Oil 274 sample is shown in Figure 11. The FTIR spectra clearly show the peak evolution of various hydrocarbons and CO_2 occurs at about 28 minutes in agreement with the mass loss results shown in Figure 9(a).

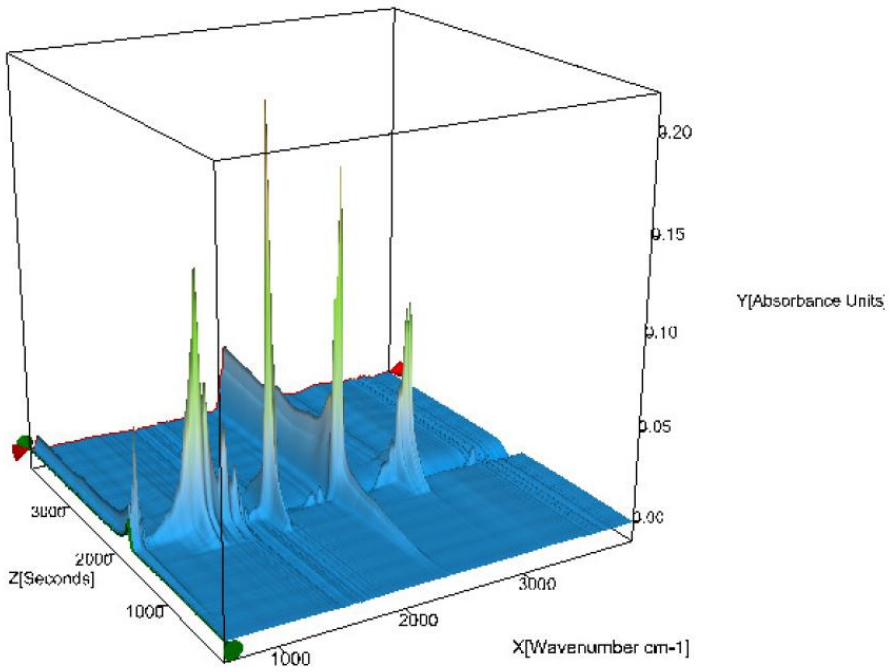

Figure 11. 3D plot of gas evolution FTIR absorbance data versus time for BP274 sample.

The FTIR spectra obtained at the time of greatest mass loss for each of the four oils investigated are shown in Figure 12(a). Each of the oils exhibited similar peaks with minor differences in relative peak heights amongst the four jet engine oils investigated. Principal components analysis was performed on the experimental FTIR data to determine the number of components most likely present in the evolved gas species from the heated engine oil samples. These results were then compared to the mass spectrometry data for verification and to determine the probable identity of the gaseous components being evolved during thermal degradation.

Figure 12(b) shows pure component spectra from the following possible constituents of the evolving gaseous mixture: methanol, formaldehyde, carbon monoxide, carbon dioxide and water. Note the strong and well identifiable CO_2 peak between wavenumbers of 2300-2400 cm^{-1}. There is no overlap between this peak and other possible species. CO_2 exhibits another peak between wavenumbers of 600-700 cm^{-1}. CO exhibits FTIR absorbance peaks between wavenumbers of 2050-2250 cm^{-1} with minimal overlap from other possible species. Peaks for methanol (CH_4O) appear at 2800-3050 cm^{-1} as well as 1000-1100 cm^{-1}. Formaldehyde (CH_2O) absorption peaks occur from 2700-3000 cm^{-1} and also from 1700-1800 cm^{-1}. Water is a strong IR absorber over a wide range of wavenumbers from 1400-2000 cm^{-1} as well as 3500-3950 cm^{-1}. Overlap of the absorption peaks due to water and methanol with formaldehyde's absorption peaks complicates evolved gas analysis when these three species may all be simultaneously present.

Principal components analysis was also applied to the FTIR spectra of gases evolved as a function of time for BP turbo Oil 2380 thermally degraded in the Oil Degradation Module shown in Figure 6(d). Initial calculations utilized simulation data sets created from pure component database spectra for comparison against the evolving gas mixtures. After using principal components regression analysis to determine likely concentrations for methanol (CH_4O), formaldehyde (CH_2O), carbon dioxide (CO_2), carbon monoxide (CO) and water vapor (H_2O) of the BP Turbo Oil 2380 time evolved samples, reconstructed prediction FTIR spectra were calculated. These reconstructed spectra were then compared to the experimentally obtained FTIR data as shown in Figure 13(a-d) for elapsed times of 10 min., 30 min., 60 min. and 90 min. The RMSE between the predicted and actual spectra for each of the time-evolved spectra were calculated to be 2.7%, 8.4%, 9.2%, and 9.0% for 10 min., 30 min., 60min., and 90 min., respectively. The average RMSE between the predicted and actual spectra for all 20 of the time evolved spectra was found to be 7.5%. The principal components analysis indicated that the following species were present in varying amounts: water vapor (H_2O), methanol (CH_4O), carbon monoxide (CO), carbon dioxide (CO_2) and perhaps formaldehyde (CH_2O) [32]. Additional work is planned using gas chromatography – mass spectrometry to further investigate and confirm these results – especially the findings regarding the presence of methanol and perhaps formaldehyde.

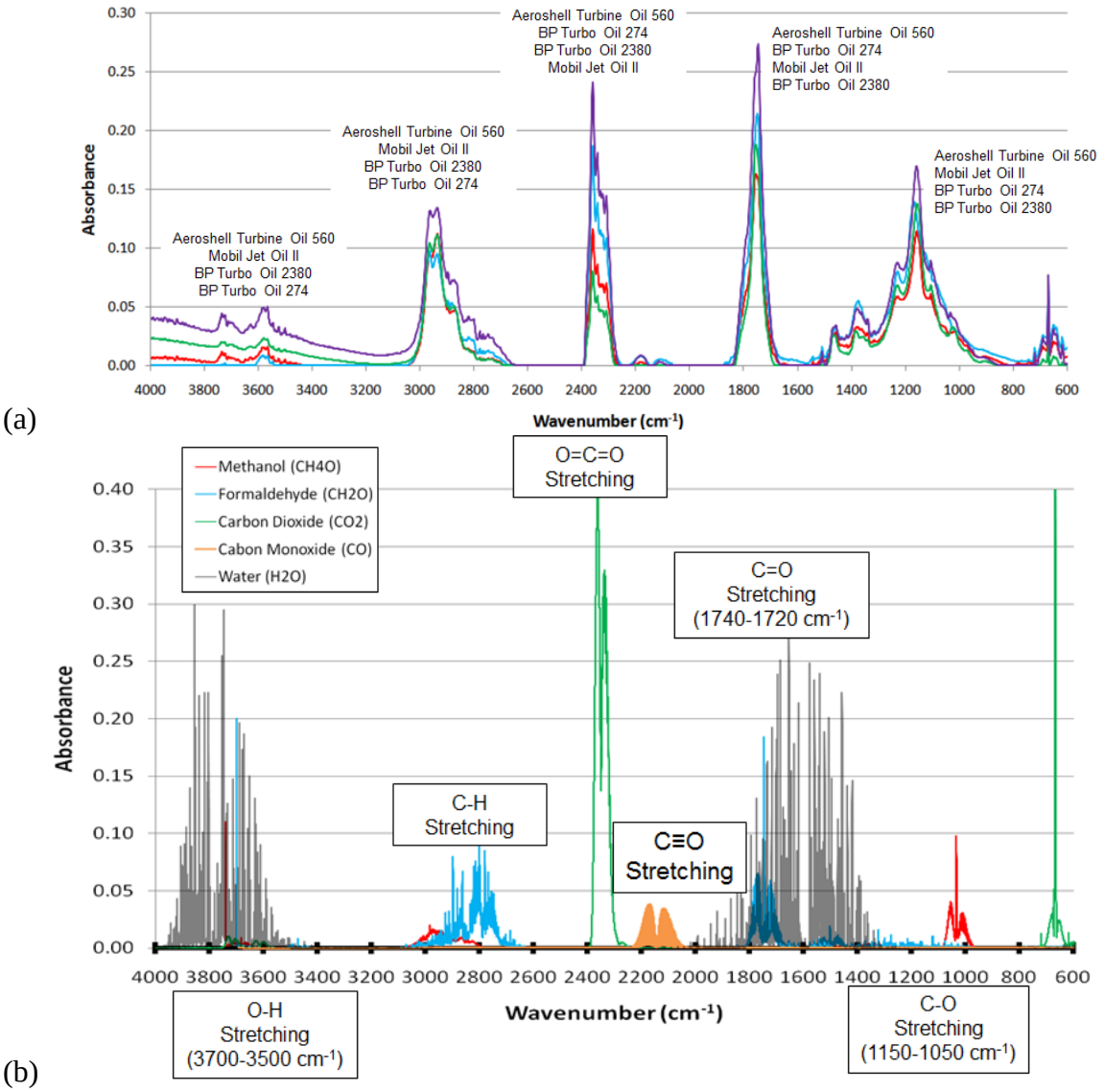

Figure 12. (a) FTIR scans of BP Turbo Oil 274(301°C), BP Turbo Oil 2380(305°C), Aeroshell Turbine Oil 560 (326°C) and Mobil Jet Oil II (307°C) at the indicated temperatures of greatest mass loss. The order of the data in each peak from each oil sample is indicated by the listing adjacent to the peak.
(b) Pure theoretical spectra from various possible components of the evolving gas mixture. The infrared bond excitation regions are also indicated.

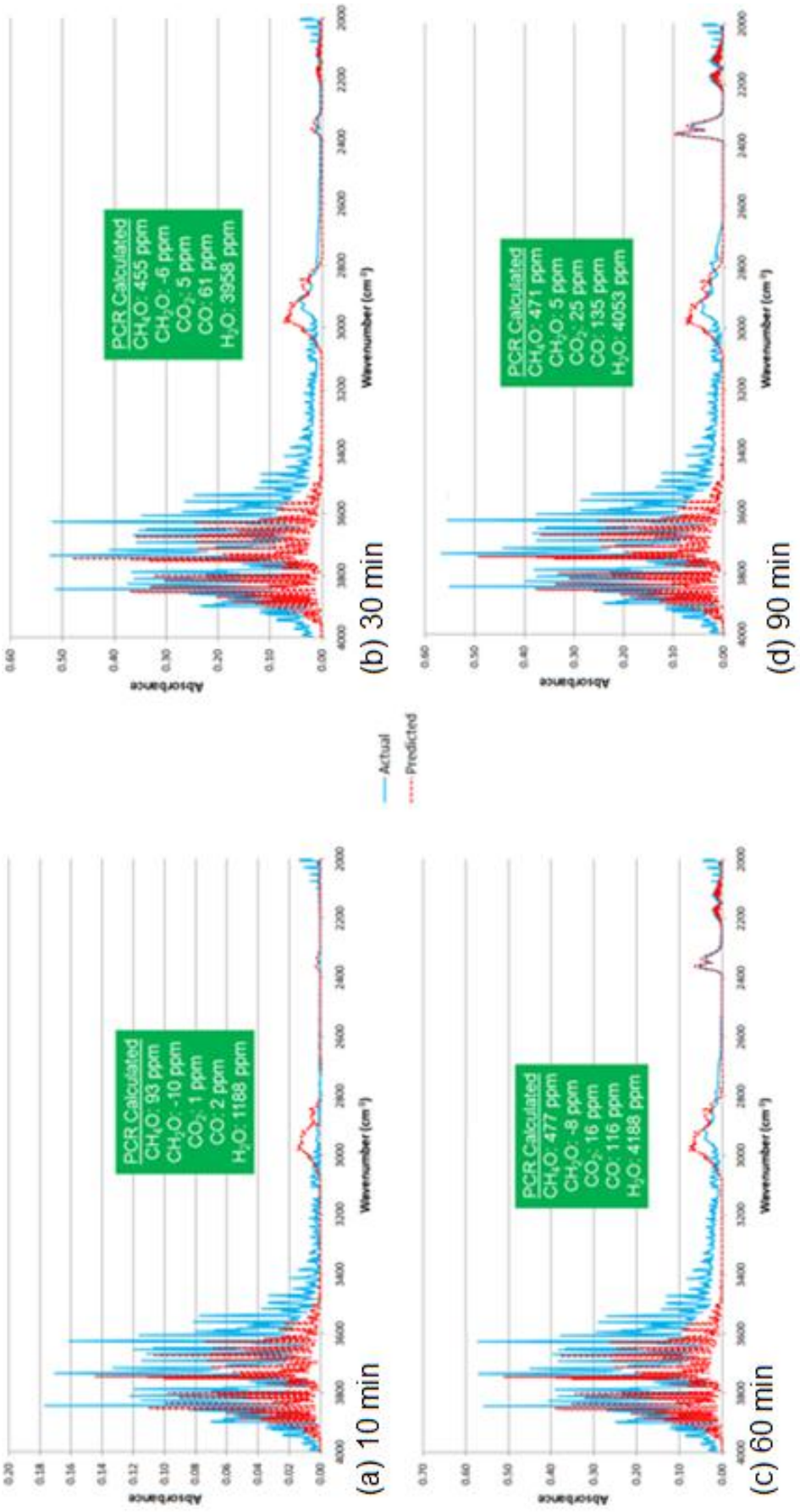

Figure 13. Experimental and calculated FTIR spectra and predicted evolved gas compositions at the times indicated during thermal degradation of BP Turbo Oil 2380. See the text for a discussion of the calculation procedures [32].

4.2 Commercial CO and CO_2 Sensor Test Results

As noted previously, NDIR-based commercial sensor technologies exist for detecting CO_2 in the air supplies of office buildings. In addition, electrochemically-based technologies are available for assessing the presence of CO from the exhaust of combustion processes. Commercial sensor systems contain all the various technologies needed to transport the test gas to the actual sensing element as well as the required electronics needed to supply system power plus acquire, condition and transmit the resultant sensor response signals. Sensor technologies developed for office buildings or garages cannot be applied to aircraft applications without being thoroughly vetted to ensure reliable performance in conditions representative of the aircraft application.

The accuracy and precision (sensitivity and detection limits) as well as calibration methods for NDIR CO_2 sensors and electrochemical CO sensors have been investigated using premixed calibration gases over a range of pressures representative of aircraft operation (Section 4.2.1). In addition, typical CO_2 and CO sensor responses due to fumes generated from thermal degradation of jet engine oil are also presented (Section 4.2.2). Issues regarding sensor selectivity, life, size, weight, cost, etc. will be explored in future work.

4.2.1 Commercial Sensors Responses to Calibration Gases

NDIR CO_2 sensors: Many commercially available NDIR CO_2 sensor technologies utilize specialized drying techniques to remove water vapor from the air. Typical sensors utilize the 4.26 μm infrared absorption band (wavenumber = 2349 cm^{-1}) of CO_2 for the measurement since that wavelength provide the least interference with the absorption bands of other gases. In addition, many commercial systems also utilize an automatic background calibration technique that presumably avoids having to actually calibrate the sensors. This method appears reasonable for office buildings that are essentially unoccupied for long periods of time (e.g., overnight, weekends). Since CO_2 is generated by building occupants, the air in office buildings should refresh during extended unoccupied periods and return to the 400 ppm CO_2 level that is typical of the overall atmosphere. The electronics in sensors that attempt to exploit this 400 ppm night-time CO_2 level automatically adjusts the calibration of the sensor to this periodically measured low level of CO_2. However, such "calibrations" could prove problematical for sensors on aircraft that do not experience such repetitive low levels of CO_2.

Figure 14 shows a typical set of commercial NDIR CO_2 sensor responses as well as the FTIR measurement during exposure to a calibration test gas of nitrogen and carbon dioxide. The overall test chamber pressure was maintained at 0.67 atm (10,780 ft equivalent altitude) and 1340 ppm CO_2. The responses of the sensors and the FTIR appear to track the slowly varying CO_2 level in the test chamber. Some sensors (A6 and A7) measured higher levels of CO_2 than the test gas composition (1340 ppm at 0.67 atm) while the other sensors indicated lower levels of CO_2 than expected. The FTIR measurement agreed most closely with the actual composition of the calibration test gas. Additional tests of these sensors indicated very repeatable responses over the range of pressures investigated. Laboratory recalibration of these NDIR sensors would likely enable very accurate and precise measurements of the calibration test gases.

The effect of pressure on sensor response was also investigated and typical results are shown in Figure 15. The theoretical pressure sensitivity of the CO_2 partial pressure for a gas composition of 1100 ppm CO_2 at 1 atmosphere (i.e., CO_2 partial pressure of 0.11 kPa) was calculated assuming ideal gas behavior. The theoretical dependence of CO_2 partial pressure upon chamber pressure (slope = -0.18) was then experimentally compared to sensor indications from a Johnson Controls CD-WA0 NDIR CO_2 sensor. As shown in Figure 18, the commercial sensor exhibited a higher sensitivity to pressure (slope = -0.24) than expected from the ideal gas law. Table V shows the pressure sensitivity of a number of additional NDIR CO_2 sensors investigated and all sensors exhibited higher sensitivity to pressure that expected. The average sensor was approximately 27% more sensitive to pressure than expected.

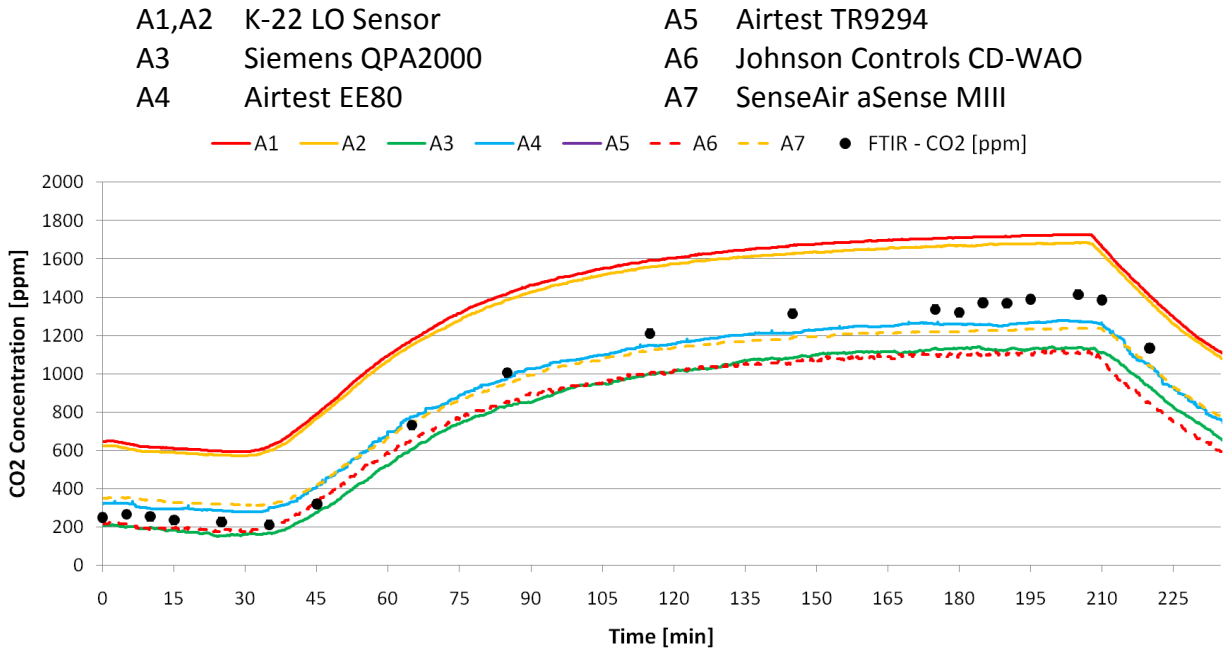

Figure 14. Laboratory FTIR and commercial CO_2 NDIR sensor responses to introduction of 1340 ppm CO_2 in nitrogen at 0.67 atm pressure in the test chamber (10,780 ft equivalent altitude). Indicated time is from the beginning of introduction of the test gas. Test gas flow stopped at 200 min.

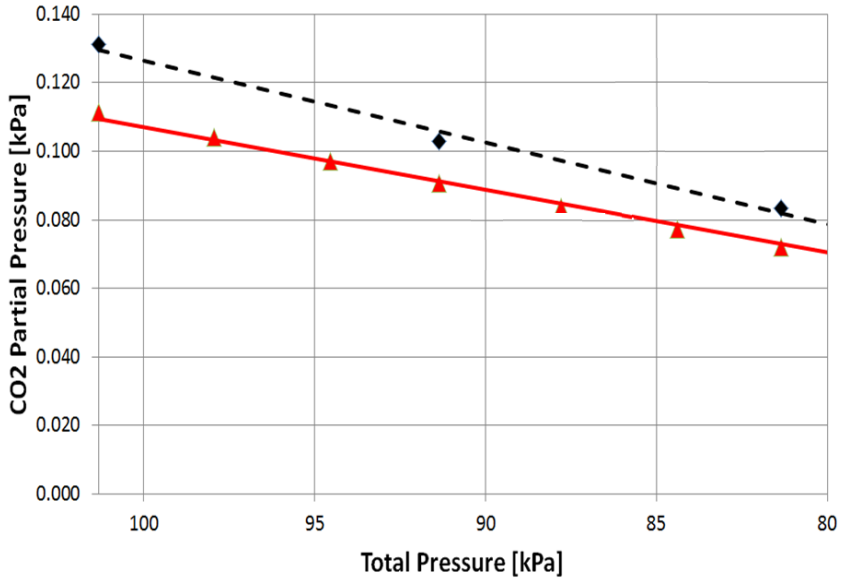

Figure 15. Theoretical pressure sensitivity (triangles) of the CO_2 partial pressure calculated assuming ideal gas behavior compared to sensor indications from a typical NDIR CO2 sensor (diamonds: Johnson Controls CD-WA0). Note that the commercial sensor exhibits a higher sensitivity to pressure than expected from theoretical considerations.

Table V
Pressure Sensitivity of Commercial NDIR CO_2 Sensors

Sensor Manufacturer	Model Number	Theoretical Slope	Actual Slope	% Difference
Expected Pressure Dependence		***-0.0018***		
AirTest Technologies	TR9290		-0.0023	27.8
AirTest Technologies	EE80-2CT3		-0.0023	27.8
Automation Components Inc.	ACI/CO2-VDC-R		-0.0022	22.2
Digital Control Systems Inc.	M307		-0.0024	33.3
Greystone Energy Systems Inc.	CDD1A2000		-0.0023	27.8
Honeywell	C7232A1016		-0.0024	33.3
Intec Controls Inc.	I-310E		-0.0026	44.4
Johnson Controls	CD-WA0-00-0		-0.0024	33.3
Senseta	4GS-1		-0.002	11.1
Siemens	QPA2000		-0.0022	22.2
Telaire	Venostat 8001		-0.0023	27.8
Telaire	Venostat 8002		-0.0022	22.2
Vaisala	GMW21		-0.0022	22.2
Veris Industries	CWE SC		-0.0024	33.3
Vulcain	90DM4SM-C-2000		-0.0022	22.2

Electrochemical CO sensors: Figure 16 compares the steady state outputs (mg of CO per m^3) of each commercial sensor against the known concentration of CO in the test chamber for binary test gases of nitrogen and CO in the test chamber pressures indicated. In the ideal case the sensors would output exactly the same CO concentration as the known concentration resulting in linear behavior as shown by the 1:1 line in Figure 16. Most sensors predicted greater amounts of CO in the test chamber at each pressure level than were actually there. Perhaps the factory calibrations were intentionally set conservatively high due to the hazards associated with CO poisoning. Examination of the results shows that each sensor demonstrated a linear response to an increase in the CO concentration. This suggests that the sensors could be recalibrated to provide a more accurate measurement of the steady state CO concentration in the test chamber.

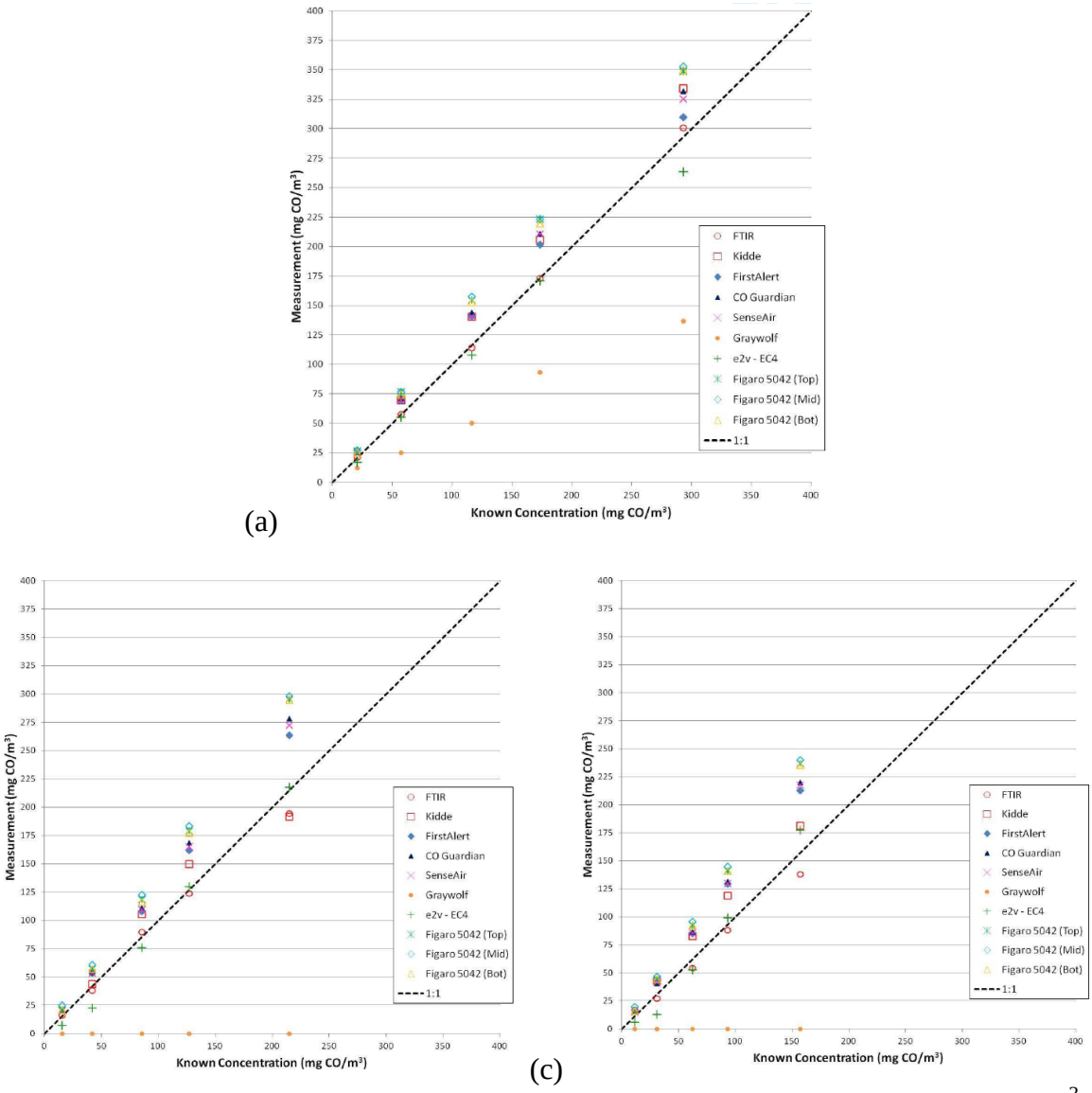

Figure 16. Experimental measurements of CO concentration in nitrogen (mg CO per m^3) for the electrochemical sensors indicated versus known concentrations in pure nitrogen test gases at the following pressures: (a) 101.3 kPa, (b) 87.5 kPa and (c) 75.3 kPa [33]

The data for the Figaro 5042 sensor are replotted in Figure 17 for nitrogen with CO at test pressures of 101.3, 87.5 and 75.3 kPa. Figure 17 clearly shows a linear response for the Figaro 5042 sensor at each of the pressures. The increasing slope of the sensor response as the pressure is reduced suggests that the accuracy of the sensors perhaps decreases slightly as the pressure decreases. However, the sensor behavior is linear and predictable.

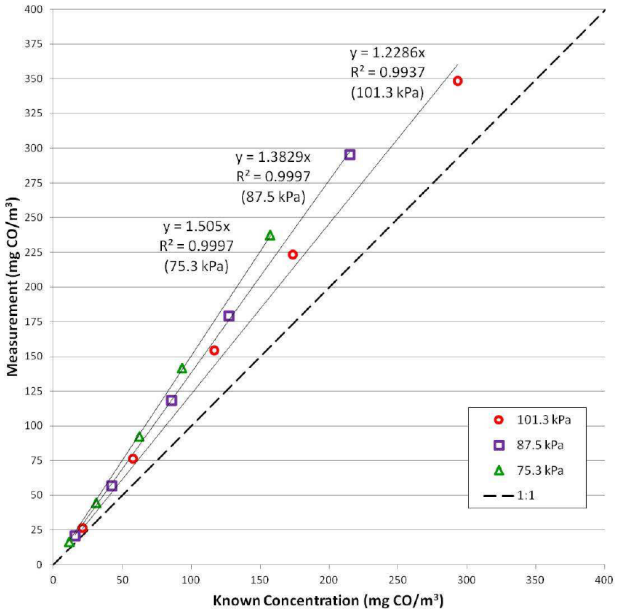

Figure 17. Figaro 5042 sensor response to nitrogen gas with the indicated known concentrations of CO at test pressures of 101.3, 87.5 and 75.3 kPa. [33]

Figure 18 presents the results of repeated experiments on the Figaro 5042 sensor for a steady-state concentration of 233 mg of CO per m^3 in nitrogen-20% oxygen at a pressure of 101.3 kPa. The Figaro 5042 sensors exhibited stable, repeatable steady-state output without any overshoot or undershoot. The responses were quite repeatable in these initial experiments. The e2v sensor demonstrated a first ordered response to an increase in the CO concentration with stable, repeatable steady-state output. Unfortunately, the Graywolf sensor malfunctioned and never responded to any of the CO inside the sensor evaluation system.

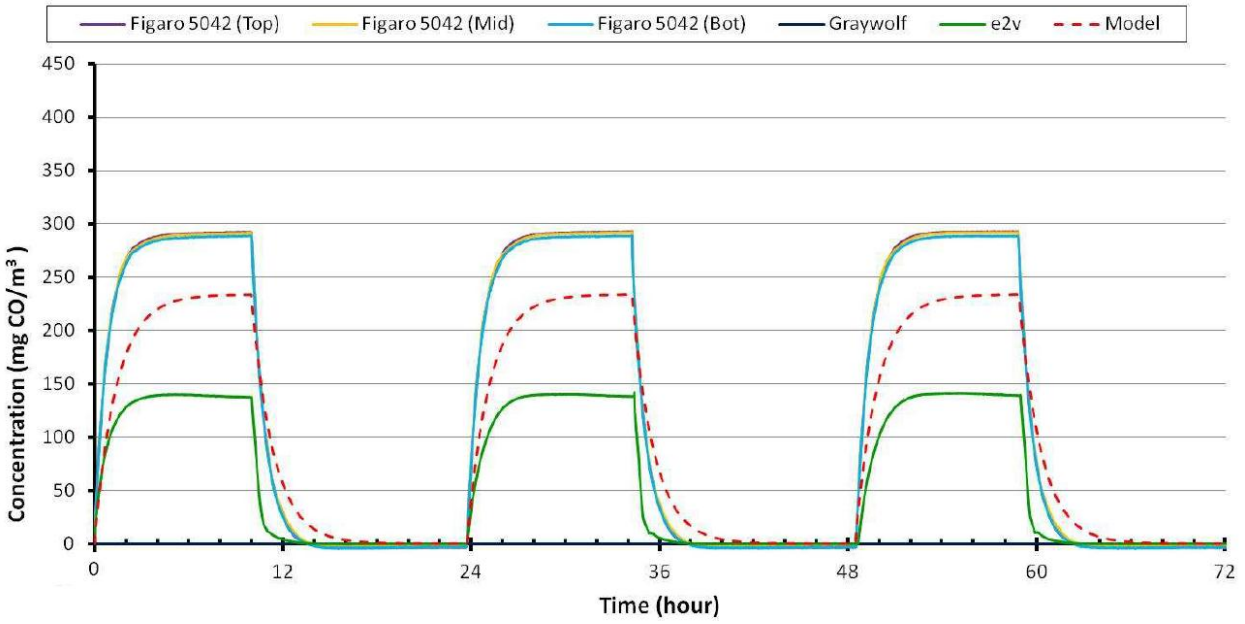

Figure 18. Three repeated transient measurements of CO concentration (known value = 233 mg CO/m^3) in simulated air (80% nitrogen and 20% oxygen) at 101.3 kPa for the electrochemical sensors indicated. The calculated transient test chamber concentration is shown by the dashed line. [33]

4.2.2 Commercial Sensors Responses to Fumes from Mobil Jet Oil II

One gram of Mobil Jet Oil II was thermally degraded in the bell jar shown previously in Figure 6(d). The furnace target maximum temperature was set to 375°C and a heating rate of 10°C/min was utilized to heat the oil sample. The oil began to lose mass after approximately 30 minutes and at a temperature of approximately 190°C. White smoke was observed at that time and the amount of smoke increased as the experiment progressed as shown in Figure 19. The oil reached and maintained a steady state temperature of 225°C during the time that mass loss and smoke generation continued. At the end of the experiment, only charred black material remained in the crucible.

(a) 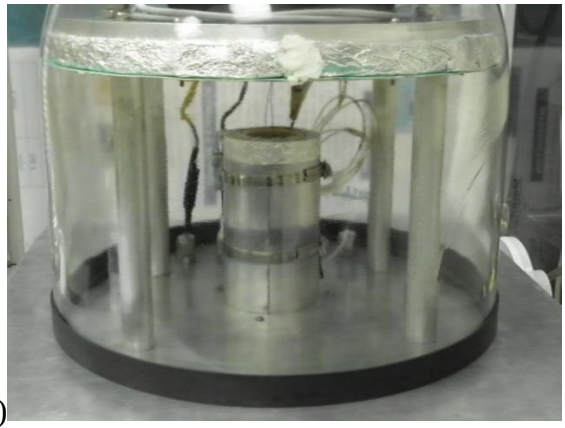 (b) 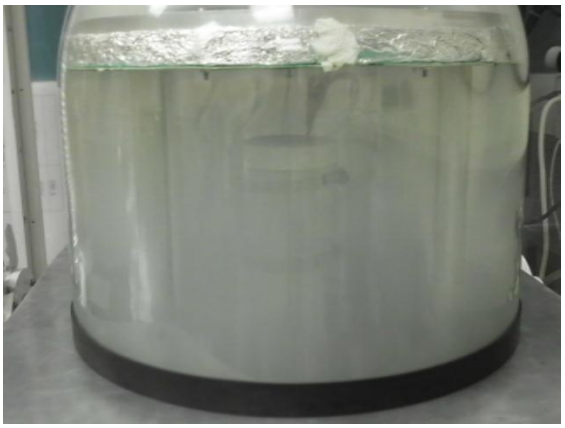

Figure 19. a) Bell jar before thermally degrading 1g of Mobil Jet Oil II; b) smoke-filled bell jar during degradation experiment. [34]

Figures 20 and 21 show the change of CO and CO_2 concentration as a function of time along with the Mobil Jet Oil II mass change. The sensors began detecting CO and CO_2 at approximately the same time that significant mass loss began (~30 minutes). The downstream FTIR began detecting changes in the air samples about 5 minutes later. The measured concentrations from the sensors and the FTIR appear to reach maximum values near the end of the thermal degradation. Interestingly, although the downstream FTIR detection of CO shown in Figure 20 began to decrease after the upstream electrochemical sensor, as expected, the FTIR detection of CO_2 began to decrease before the upstream NDIR CO_2 sensor as shown in Figure 21. This behavior may be due to smoke coating the NDIR sensor optics during the experiment and is under further investigation.

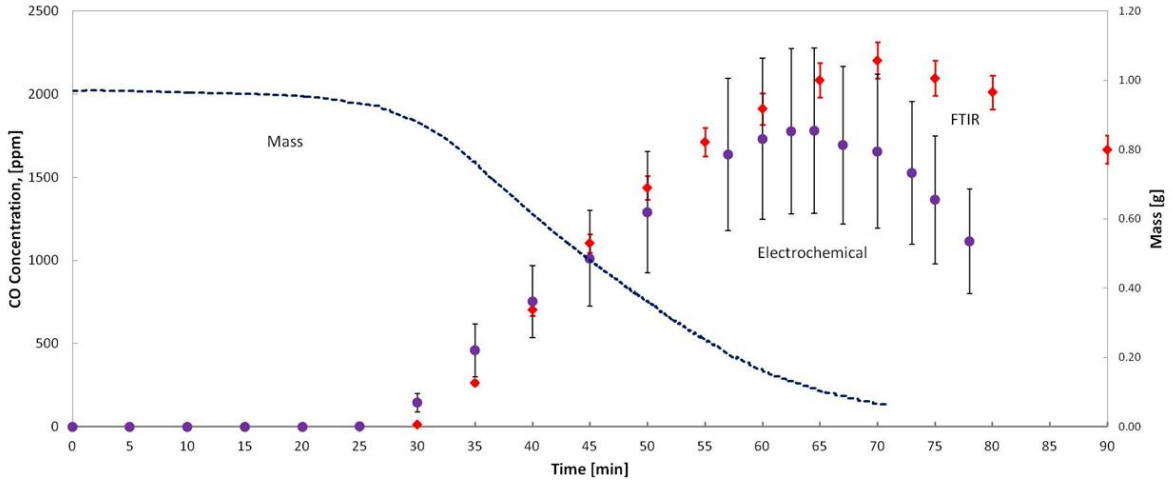

Figure 20. Plot of the change in CO concentration as a function of time as measured by the TGS5042 sensor (circles) and the FTIR (diamonds) and the mass (dashes) as a function of time. [34]

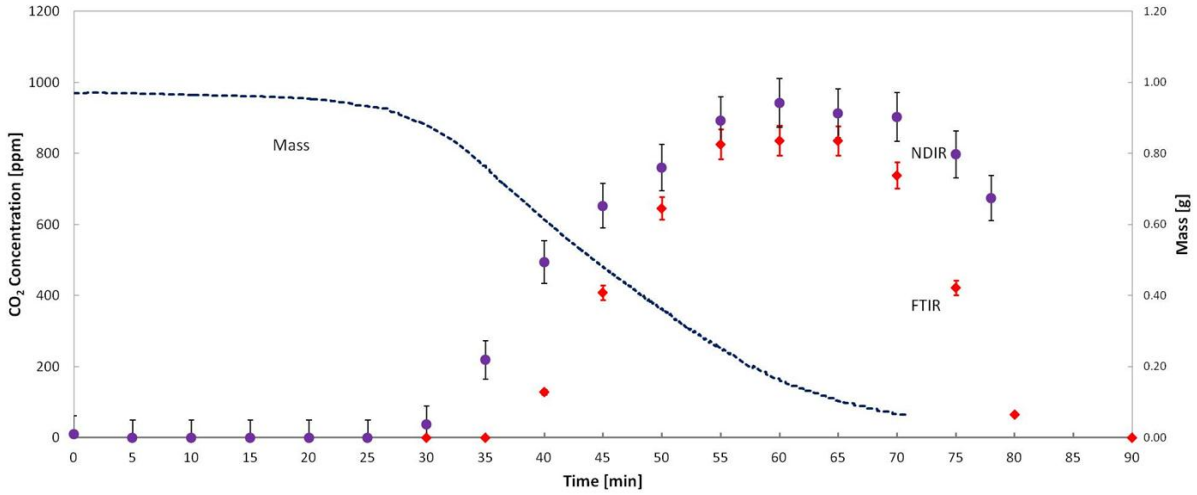

Figure 21. Plot of the CO_2 concentration as a function of time as measured by the EE80 (circles) and the FTIR (diamonds) and the mass (dashes) as a function of time. [34]

4.3 TCP Sensor Developments

To test the ability of the tricresyl phosphate (TCP) sensor system discussed in Section 3.2.2 to detect TCP in gas, several samples of vapor phase TCP were produced by evaporation and collected with the automatic TCP sampling system. Different concentrations of TCP (0 as control, 2.5, 10, 50, and 200 nM) in methanol were evaporated by bubbling nitrogen gas at 1.1 L/min through the methanol solution for 10 min. During the last 5 min of bubbling, 220^{o}C nitrogen gas at 220^{o}C was used to ensure that all the TCP was evaporated. The total nitrogen gas volume equaled 11 L giving TCP concentrations of 0, 5, 20, 100, and 400 ppb. All nitrogen containing TCP samples were blown through the alkaline powder catalyst column. Finally 3 mL of Na_2HPO_4/KH_2PO_4 (0.2 M/0.2 M final concentrations) and 10 mM NaCl buffer was flushed through the powder column to collect hydrolyzed products. All sample preparation and collection steps were accomplished with an automated custom TCP sampling system. By these processes, TCP gas samples were converted to liquid samples containing corresponding concentration of cresol, making it possible to be detected using the electrochemical sensor discussed in Section 3.2.2.

The flow injection results from TCP converted samples are shown in Figure 22. The concentration of TCP in the gas is seen to be linear over the gas concentration range of 5 to 400 ppb. The lower concentration part of Figure 21 is enlarged and shown in the inset of Figure 21 (0, 5 and 20 ppb). These results confirm the capability of the laboratory system to detect TCP in gaseous samples. The lower detection limit is estimated as 5 ppb in gas.

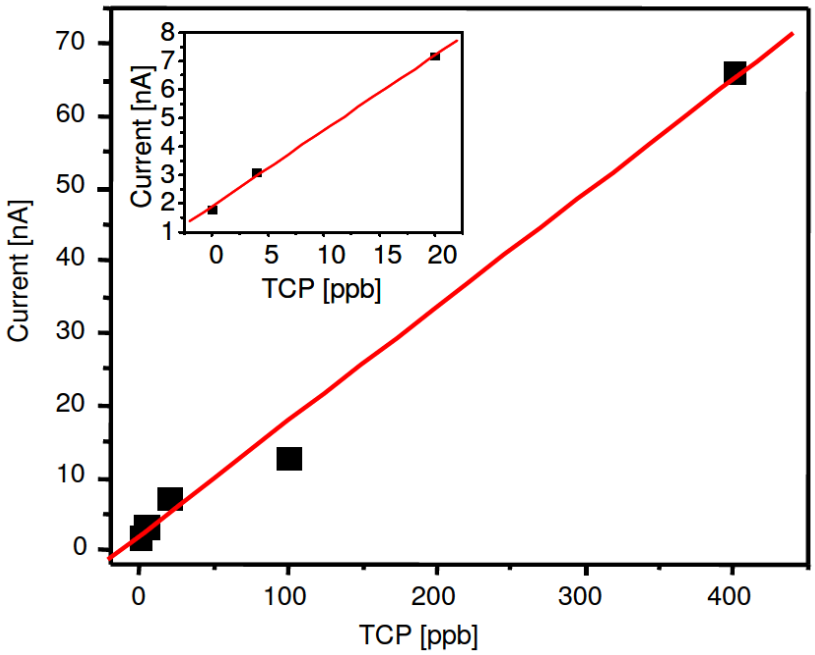

Figure 22. Calibration curve of amperometric results of TCP converted samples. Linear concentration range is from 5 ppb to 400 ppb in gas. Inset figure shows low concentration range (5 and 20 ppb). 0 ppb means sample was from methanol without TCP, acting as control sample.

To further test the ability of the system to detect TCP in air from more realistic samples due to jet engine oil, 4 µL of BP2380 and BP 274 oil samples were mixed in methanol and then processed through the detection system (as described above). BP 2380 jet engine oil contains a maximum of 5% TCP while BP 274 jet engine oil is free of TCP additives. The concentrations of TCP in the air stream were calculated to be 600 ppb (BP 2380) and 0 ppb (BP 274). The peak electrochemical current response from the BP 2380 sample was 28.5 nA (std. dev. = 1.40 nA) while the BP 274 oil sample exhibited a peak electrochemical current of only 3.78 nA (std. dev. = 0.06 nA). The response of the sensor to the TCP containing oil vapor sample was thus approximately an order of magnitude higher than for the TCP-free BP 274 oil vapor sample.

4.4 Particulate and Ultrafine Sensor Test Results

The bleed air contaminant simulator built for the previous "Filter" project is being used to characterize the nature of airborne contaminants generated in oil-based contamination events. As part of this effort, the nature of the particulate sizes and distributions are being measured for different conditions as it is believed that a particulate sensor has the potential to be part of an effective bleed air contamination detection system. A diagram of the bleed air simulator at Kansas State University is shown in Figure 23.

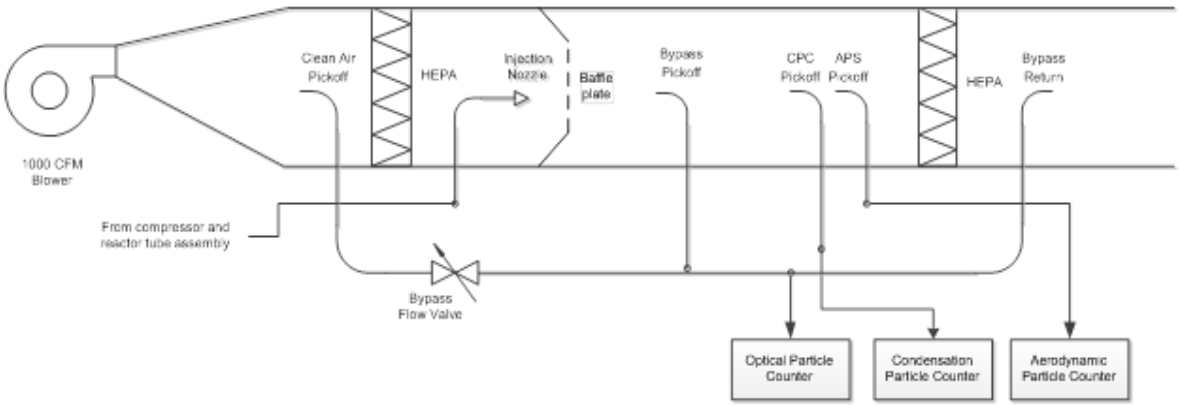

Figure 23. Kansas State University Bleed Air Contamination Simulator.

Three different instruments are being used to measure particle numbers and sizes. The first is an "Aerodynamic Particle Sizer" (APS). The particular instrument being used is the TSI Model 3321 APS. This instrument measures aerodynamic diameter by recording the time of flight of particles as they are accelerated through a nozzle. Particle size is binned into 52 channels from approximately 0.5µm to 20 µm. This instrument is noted for providing high quality size distribution information.

The second instrument is a "Condensation Particle Counter" (CPC). The particular instrument being used is the TSI Model 3781. The CPC allows particles as small as 6 nm to be counted, thus greatly extending the range of particle sizes detected beyond what the APS can detect. The CPC condenses moisture onto the particles to grow them to a size that can be detected. Consequently, there is no size distribution information, only total particle counts.

The third instrument is an "Optical Particle Counter" (OPC). The particular instrument being used is the Climet Spectro 0.3. The OPC calculates particle size and concentration by measuring the intensity of light scattered by the particles. Particle size is binned into 16 channels from 0.3µm to 10µm.

Three separate but otherwise identical APSs are available for comparison to verify that the results are reliable. At this point, we are having some difficulty reconciling OPC and APS measurements and only APC and CPC data are reported at this time. The data collected to date are strictly preliminary. A summary of the data may be found in Table VI. Figure 24 shows the size distributions for the different temperature conditions indicated.

From these results it can be seen that the APS counts decrease as temperature increases while the CPC counts increase significantly as temperature increases. Although one could speculate as to the mechanisms that lead to these results, we will not do so until further data are collected. However, an increase in ultra-fine particles as the process temperature reached the pyrolysis point was predicted. Whether or not that we are seeing smoke at this point -- or some other phenomena -- is not yet clear.

Table VI
Summary of Particle Measurements

Parameter	Units	Test 1	Test 2	Test 3	Test 4
Reactor Tube Temp	°C	104.8	199.4	244.5	276.7
Comp Pressure	psi	31	29	30	32
CPC Concentration	counts/cm3	34,202	63,809	98,066	124,917
APS Concentration	counts/cm3	885.0	1961.3	767.0	120.8
Mean Aero Diameter	µm	0.71	0.71	0.69	0.68

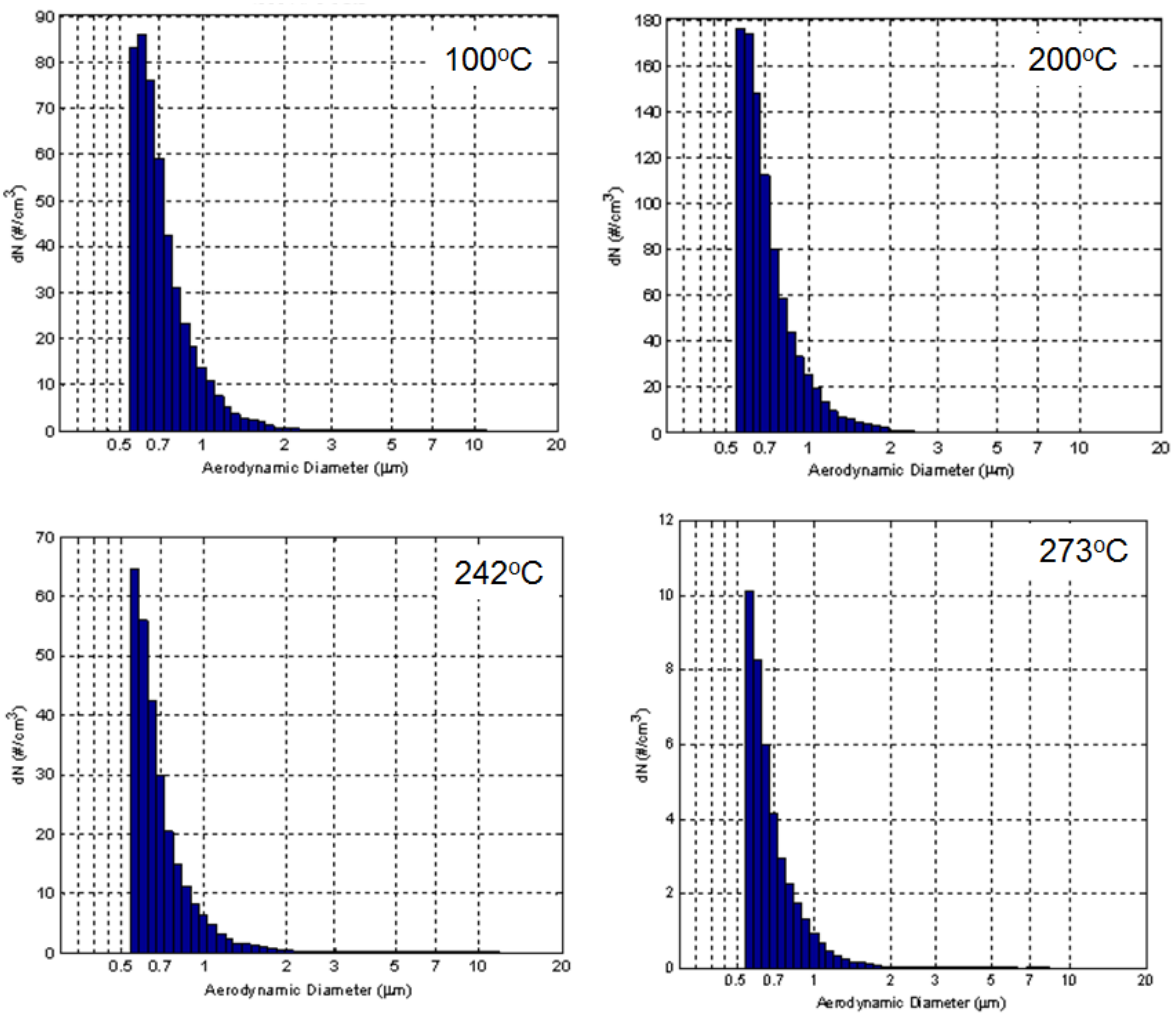

Figure 24. Particle size distributions at the indicated test temperatures as measured by APS.

4.5 Wireless Sensor Network Field Test in an Aircraft Cabin Mock-up

Test Series 2 of the wireless sensor network testing in the KSU B767 cabin mock-up was composed of four test runs that focused on CO_2 measurements. During the first two runs only CO_2 was flowed into the cabin. During Runs 3 and 4, CO_2 was inserted, passenger dummy heaters turned on, and cabin humidifiers were cycled. Table VII shows the experimental timeline.

As seen in Figure 25, CO_2 concentrations were well distributed through the cabin. Since the CO_2 was flowed into the front of the cabin, the highest concentration of CO_2 was seen nearest the front of the cabin. The concentration decreased toward the rear of the cabin. From Figure 23, we see that during the last two runs (which included humidity and temperature variations) sensor node U2 showed a significantly higher concentration of CO_2 than the other tests. Which effect (increased heat or humidity) may have caused this response is not clear.

Table VII

Wireless Sensor Network Field Test - Series 2 Timeline

Time	Event	Description
18:55:00	Start of Test Series 2	All units power cycled. Note: Turning the CO_2 on and off does not require any doors to open in the cabin.
UU:UU:UU	Node reset	CO_2 was flowed but Unit 3 had to be reset because it stopped sending data.
19:05:00	Started Run 1	Flowed CO_2
19:28:00	Stopped Run 1	Stopped CO_2
19:43:20	Started Run 2	Flowed CO_2
20:08:00	Stopped Run 2	Stopped CO_2
20:12:00	Started Heaters	Passenger dummy heaters started
20:22:00	Started Run 3	One occupant entered and started humidifiers.
20:22:10	Closed Door	Closed door 2. Started CO_2.
20:57:00	Stopped Run 3	All humidifiers turned off and CO_2 stopped.
21:13:00	Started Run 4	Door 2 opened, humidifiers started.
21:13:10	Door Closed	Door 2 closed. CO_2 started.
21:37:00	Stopped Run 4	All humidifiers turned off and CO_2 stopped

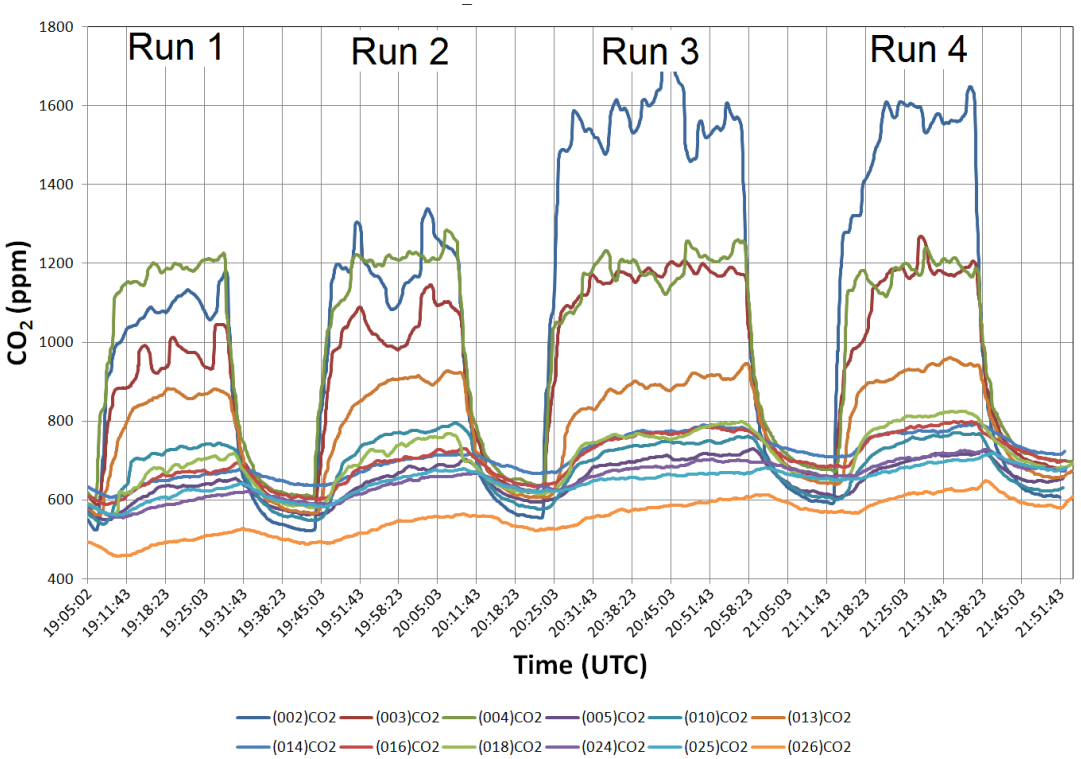

Figure 25. Wireless sensor network field test results for CO_2 sensors.

4.6 Preliminary Data Mining Results from the FAA SDRS and NASA ASRS Databases

Murawski's and Supplee's results[9] were extended by searching all of the Service Difficulty Reports (SDRs) in the FAA SDRS database and the documents in the NASA ASRS for entries containing the same keywords as Murawski and Supplee chose. As the Structured Query Language (SQL) database file for the SDRs was available, this task was accomplished through a SQL query using the REMARK LIKE terms and the % wildcard character to grab all entries related to the keywords. The ASRS's database file could not be directly manipulated in this way. Instead, the web interface was utilized for limited queries using an SQL like language. However, in this manner, only 5000 entries be drawn out of the ASRS database at a time. The AND and OR terms, in addition to the % wildcard character, was used to draw out the same keywords as the query made on the SDRS database. These entries were compiled in four year intervals (data from 2008 – 2012, etc.) and then concatenated together due to the 5000 entry limit. 17,878 cabin air quality related reports were pulled from the SDRS database while 10,644 cabin air quality related reports were pulled from the ASRS database. This provided a data set much larger and potentially more representative of air cabin quality events in general than the more limited dataset of 470 reports analyzed by Murawski and Supplee.[9]

The total frequency of each of the keywords in the dataset was examined first. The complete set of SDRs provides the most entries for almost every keyword and the most entries overall. This indicates that there are far more airline self-reports to the FAA than reports made by airline personnel to the NASA ASRS database. However, the two datasets were not compared for overlapping documents or for documents contained in one database and not the other. Such additional research is planned.

The portion of entries containing each keyword remained fairly stable across all of the sets of data. However, there were a few exceptions. The keyword phrase "oily smell" was found much more frequently in Murawski and Supplee's data.[9] This could be due to their small sample size. Murawski and Supplee collected SDRs and AIDS data for a little over a year, whereas the whole SDR database stretches back to 1995 and the ASRS data began being reported in 1988. Interestingly, the keyword phrase "oil leak" was found comparatively infrequently in the ASRS data.

The number of entries present for each year in each database was counted using SQL queries. The ASRS database contained consistently fewer entries than the number of air cabin quality entries found in the SDRs for each year. The only exception was that of the most recent year. Not all SDRs have been added to the database for the current year while data have been added to the ASRS database in a much more timely fashion. It is also interesting that the number of incidents reported in each database has remained relatively similar from year to year. Nevertheless both databases indicate that the trend is for cabin air quality incidents to slightly increase over time. This slight uptrend was broken in the years after September 11, 2001, where the number of consumer flights decreased dramatically overall.

The top 4 aircraft types associated with bleed air events in the SDRS database appear to be the following: CL-600-2B19 (aka Bombardier CRJ100 and CRJ-200), Embraer 145LR, MD-82 and MD-88. The top 4 aircraft types associated with bleed air events in the ASRS database appear to be the following: Boeing 757, MD-80 Series, Boeing 737 and Airbus 320. These are preliminary data and have not yet been normalized with respect to the total number of aircraft in operation, the total number of takeoffs, etc. Such additional analysis is planned.

5.0 Summary

Principal components analysis/regression techniques have been successfully applied to Fourier Transform Infrared spectroscopy data of gases evolved from thermally degraded jet engine oils. These analyzed gases consisted of complex mixtures of carbon monoxide (CO), carbon dioxide (CO_2), methanol (CH_4O) and water (H_2O). Additional work is planned using gas chromatography – mass spectrometry to further investigate and confirm these results – especially the findings regarding the presence of methanol and as well as to look more closely for formaldehyde (CH_2O).

Sensing of carbon dioxide (CO_2) and carbon monoxide (CO) via non-dispersive infrared technology and electrochemical sensors, respectively, are widely used in commercial applications. Both methods offer considerable promise for aircraft measurements of these same gaseous contaminants. However, existing sensor packaging and maintenance/calibration methods must be adapted to the unique environment and more stringent performance requirements anticipated for aircraft. In addition, research into the response times of the sensors is critical to ensure that transient bleed air events can be quickly and reliably detected. Finally, the potential application of catalytic bead sensor technology to characterize the presence of unburned hydrocarbons during incomplete pyrolysis of jet engine oil during bleed air events must also be evaluated.

Computerized data mining techniques were utilized to replicate and improve upon the results of previous researchers (i.e., Murawski and Supplee [9]) by expanding the data set used to the entirety of the FAA SDRS and the NASA ASRS databases. The preliminary findings are promising and further research may lead to the creation of association rule classifiers for use in rigorously characterizing cabin air quality incidents.

Wireless sensor networks can provide the necessary coverage and cooperation to effectively monitor air quality sensor systems in aircraft bleed air supplies and airliner cabins. A prototype of such a system has been successfully tested in a Boeing 767 mock-up cabin. The wireless sensor network was shown capable of monitoring multiple environmental variables, and providing real-time, correlated data and represents a new tool that will improve our ability to characterize highly dynamic environmental control systems on aircraft.

6.0 Acknowledgments

This project was funded by the U.S. Federal Aviation Administration (FAA) Office of Aerospace Medicine through the National Air Transportation Center of Excellence for Research in the Intermodal Transport Environment (RITE), Cooperative Agreements 07-C-RITE and 10-C-RITE. Although the FAA has sponsored this project, it neither endorses nor rejects the findings of this research.

7.0 References

[1] NRC (National Research Council); 2002, The Airliner Cabin Environment and the Health of Passengers and Crew, Washington, DC, National Academy Press.

[2] "De-icing solution sends air crew members to hospital," *CNN*, 24 Dec 2008.

[3] Crane, Charles R., Sanders, Donald C., Endecott, Boyd R., Abott, John K., "Inhalation Toxicology: III Evaluation of Thermal Degradation Products from Aircraft and Automobile Engine Oils, Aircraft Hydraulic Fluid, and Mineral Oil," FAA-AM-83-12, 1983.

[4] Van Netten, Chris, "Aircraft Air Quality Incidents, Symptoms, Exposures and Possible Solutions," in Air Quality in Airplane Cabins and Similar Enclosed Spaces, Hdb Env. Chem. Vol. 4, Part H (Springer, Berlin) 2005, pp. 192-210.

[5] Shayne, B., "Plane with sick passengers had air contamination before," *WCNC*, 20 Jan 2010.

[6] Abou-Donia, M.B., "Organophosphorous ester-induced chronic neurotoxicity," Arch. Environ. Health, 2003, Vol. 58, pp. 484-497.

[7] Winder, Chris and Balouet, Jean-Christophe, "The Toxicity of Commercial Jet Oils," Environ. Res. A, 2002, 89, pp. 146-164.

[8] Watson, Jean; 2009, personal communication.

[9] J.T.L. Murawski, J.T.l. and Supplee, D.S., "An Attempt to Characterize the Frequency, Health Impact and Operational Costs of Oil in the Cabin and Flight Deck on U.S. Commercial Aircraft," J. ASTM Intnl , 2008, Vol. 5, No. 5, Paper ID JAI101640.

[10] Department of Transportation, Bureau of Transportation Statistics, http://www.bts.gov/publications/national_transportation_statistics/html/table_01_37.html, accessed February 3, 2012

[11] "Air Quality within Commercial Aircraft," ANSI/ASHRAE Standard 161-2007, American Society of Heating, Refrigerating, and Air-Conditioning Engineers, 2008, Atlanta, GA.

[12] Hunt, Elwood H., Reid, Don H., Space, David R. and Tilton, Fred E., "Commercial Airliner Environmental Control System," Aerospace Medical Association Annual Meeting, 1995, Anaheim, CA, USA.

[13] Jones, Byron, personal communication, 2011.

[14] van Netten, C., Leung, V., "Hydraulic Fluids and Jet Engine Oil: Pyrolysis and Aircraft Air Quality," Archives of Environmental Health, 2001, 56(2): p. 181-186.

[15] van Netten, C., Multi-elemental Analysis of Jet Engine Lubricating Oils and Hydraulic Fluids and Their Implication in Aircraft Air Quality Incidents., The Sci. of the Total Environ., 1999, 229, p. 125-129.

[16] van Netten, C., Leung, V., "Comparison of the Constituents of Two Jet Lubricating Oils and Their Volatile Pyrolytic Degradation Products," Applied Occupational and Environmental Hygiene, 2000, 15(3): p. 277-283.
[17] Crane, C.R., Sanders, D.C., Endecott, B.R., Abbott, J.K., "Inhalation Toxicology: III. Evaluation of Thermal Degradation Products from Aircraft and Automobile Engine Oils, Aircraft Hydraulic Fluid and Mineral Oil," FAA Civil Aeromedical Institute, FAA-AM-83-12, 1983.
[18] Bartl, P., Volkl, C., Kaiser, M., "Chemical Characterization of Polyol Ester Aviation Lubricant Residues," J. Synthetic Lubrication, 2008, 25, p. 1-16.
[19] Jones, E., "The pellistor catalytic bead sensor," in Solid State Gas Sensors, Moseley, P.T. and Tofield, B.C., Eds., 1987, Institute of Physics, Bristol, UK, p. 17-31.
[20] Korotcenkov, G., "One-electrode Semiconductor Gas Sensors," in Science and Technology of Chemiresistor Gas Sensors," Aswal, D.K. and Gupta, S.K., Eds, 2007, Nova Science Publishers, New York, USA, p. 95-145.
[21] Chou, J., Hazardous Gas Monitors, 1999, McGraw Hill, New York, USA, p. 37-41.
[22] Kaur, M., Aswal, D.K., Yakhmi, J.V., "Chemiresistor Gas Sensors: Materials, Mechanisms and Fabrication," in Science and Technology of Chemiresistor Gas Sensors," Aswal, D.K. and Gupta, S.K., Eds, 2007, Nova Science Publishers, New York, USA, p. 33-93.
[23] Stetter, J.R., Li, J., "Amperometric Gas Sensors – A Review," Chem. Rev., 2008, 108, p. 352-366.
[24] Fergus, J.W., "Solid electrolyte based sensors for the measurement of CO and hydrocarbon gases," Sensors and Actuators B, 2007, 122, p. 683-693.
[25] Fergus, J.W., "A review of electrolyte and electrode materials for high temperature electrochemical CO2 and SO2 gas sensors," Sensors and Actuators B, 2008, 134, p. 1034-1041.
[26] Verner, P., "Photoionization detection and its application in gas chromatography," J. Chromatography, 1984, 300, p. 249-264.
[27] Shrestha, S.S. and Maxwell, G.M., 2009, "Product Testing Report – Wall Mounted Carbon Dioxide Transmitters," National Building Controls Information Program, Iowa Energy Center (Ankeny, IA).
[28] Shrestha, S.S. and Maxwell, G.M., 2009, "An experimental evaluation of HVAC-grade carbon dioxide sensors: Part 1, test and evaluation procedure," ASHRAE Transactions, 115(2).
[29] Shrestha, S.S. and Maxwell, G.M., 2010, "An experimental evaluation of HVAC-grade carbon dioxide sensors: Part 2, performance test results," ASHRAE Transactions, 116(1).
[30] Shrestha, S.S. and Maxwell, G.M., 2010, "An experimental evaluation of HVAC-grade carbon dioxide sensors: Part 3, humidity, temperature and pressure sensitivity test results," ASHRAE Transactions, 116(1).
[31] Beta, I.A., "TGA Measurements of Oil Samples with Evolved Gas Analysis by FTIR and MS," 2011, Report No. 621002184, NETZSCH Instruments North America, LLC (Burlington, MA).
[32] Haney, R.L., "Principal Component Analysis for Enhancement of Infrared Spectra Monitoring," 2011, Ph.D. Dissertation, Auburn University, Auburn, AL.

[33] Andress, J.R., "Evaluation and Analysis of Commercially Available Electrochemical Carbon Monoxide Sensors for Aircraft Applications," 2012, M.S. Thesis, Auburn University, Auburn, AL.
[32] Neer, R.L., "Development of a Laboratory Apparatus to Study the Thermal Degradation Behavior of Jet Engine Oils," 2012, M.S. Thesis, Auburn University, Auburn, AL.